Chapter 7

Applications

In this chapter the previously described finite volume framework, in the form of the three dimensional engineering software PHYSICA [24], is employed in the simulation of the shape casting of metals, which involves complex thermo-mechanical behaviour.

This is an extension to the research performed using UIFS, where a linear elastic material behaviour was also assumed [42] and further research where an elasto-visco-plastic material behaviour was assumed [89].

Initially, PHYSICA is employed to simulate the gravity die casting of a hollow aluminium cylinder and, finally, the sand casting of an aluminium test bar.

7.1 Shape casting of metals

In basic terms, a shape casting process is one in which a supply of liquid metal, of appropriate composition, is prepared, poured into a mould and then allowed to solidify [27, 15]. Heat transfer occurs from the molten metal alloy to the mould and in most cases from the mould to the environment.

A number of shape casting processes are generally described in this manner, each with their own particular advantages and disadvantages. The foundry engineer can select a suitable casting process for a component, by offsetting geometrical accuracy and/or structural soundness required for the component against the relative cost of a particular casting process. Until recently the foundry engineer relied heavily upon personal expertise and accepted working practices. In the advent of the cheaper and more powerful desktop computer, the possibility of realistic simulation software for casting processes as an aid to the foundry engineer is now becoming feasible.

7.1.1 Shape casting processes

The shape casting processes that have been studied and modelled in this thesis are those typically associated with foundries and can be briefly described as follows.

7.1.1.1 Die casting

Die or permanent mould casting involves a reusable mould, consisting of a highly conducting metal, typically tool steel [27, 15]. As the mould is highly conducting, the process furnishes castings which have undergone particularly rapid freezing, and consequently exhibit particularly fine microstructures [27]. With regard to mould filling two methods are generally employed in die casting, pressure die casting [15] and gravity die casting [82, 15]. The former involves the pressurized injection of the molten metal into the mould and is not simulated in this research, while the latter simply involves the pouring of the molten metal alloy into the mould under the action of gravity and is simulated in this thesis, as experimental data is available for the cooling, solidification and deformation [82]. Additionally, the mould is not gas permeable and for this reason the process can be more prone to porosity formation, unless precautions are taken such as performing the filling process in a vacuum [15].

7.1.1.2 Sand casting

Sand casting involves a non-reusable sand mould, which is generally chemically bonded or clay bonded (Green Sand Casting) [15]. The mould is particularly deformable and is a very poor conductor [15]. The rigidity of the sand based mould is dependent upon the bonding of the sand, for clay bonded sand the moulds are less rigid, while for chemically bonded sand the moulds are more rigid [15]. The process furnishes castings which have undergone prolonged freezing and consequently exhibit coarser microstructures [27]. Additionally the mould is gas permeable, which can reduce the amount of porosity formation in the cast [27, 15].

7.1.1.3 Investment casting

Though the process is not modelled in this research, higher precision castings can generally be achieved using the investment casting process, where particularly rigid and precise ceramic moulds are utilised [27, 15]. A wax pattern is shaped for the mould using extremely accurate and reusable metal dies and then a ceramic mould is produced from the wax pattern [15, 27].

7.1.2 Simulation of shape casting processes

Over the last 10 to 15 years a large amount of research effort has been employed in the development of physically accurate software tools for the complete simulation of the metals casting process [25, 92], with the ultimate aim being a useful computational tool for the foundry engineer. To be of major use to the foundry engineer, the simulation software must be tolerably accurate, within a reasonable computational time. This generally requires a flexible software framework which can be extended in a modular fashion depending upon the physical nature of the particular casting simulation required [25, 3].

A number of casting simulation software tools have been developed from the previously

mentioned research. ProCAST [96], MAGMAsoft [64] and THERCAST3 [12, 67] to name but a few, though at present the simulation packages available are generally of limited scope with regard to their overall modelling capability of the complete casting process.

The MAGMAsoft software [64] is a consequence of the research performed by Hattel and Hansen [48, 47, 46] as previously discussed in section 1.2.1. The software offers the simulation of mould filling and solidification by heat conduction only, in conjunction with a three dimensional finite difference analysis of the thermo-elastic equations using a staggered grid, which can be interpreted as applying a cell-centred FVM on a structured mesh as indicated in section 1.2.1. Though as yet, the solid mechanics is not fully integrated into the software MAGMAsoft [47].

The ProCAST software [96] is a well established commercial package that offers a wide range of functionality, including the simulation of mould filling, solidification by heat conduction and radiative heat transfer, in conjunction with the three dimensional mechanical analysis of non-linear material behaviour in a loosely coupled fashion [96]. The software has been developed in a FE framework [96].

The THERCAST3 software is a consequence of the research performed by Bellet et al [12, 67, 13]. At present the software offers the simulation of solidification by heat conduction only, in conjunction with a three dimensional analysis of the non-linear material behaviour in a loosely coupled fashion [12, 67, 13]. Again, the software has been developed in a FE framework [12, 67, 13].

7.1.3 Dual thermo-mechanical coupling

During the shape casting process coupled thermo-mechanical behaviour occurs. The molten metal is initially in contact with the mould and a thermal resistance can be associated with the casting/mould interface, at this stage of the process, due to the rugosity of the mould surface [29]. As the casting solidifies, due to heat transfer to the mould, gap formation can occur at the casting-mould interface and the thermal resistance will increase as a function of the gap. In this manner the thermo-mechanical process exhibits dual coupling.

7.1.3.1 Casting/mould gap formation

The variation of the heat transfer coefficient associated with the casting/mould interface during the casting process has been commented upon by a number of researchers [42, 67, 12, 27]. With regard to die casting the thermal resistance due to the gap formation is highly effective due to the high conductivity of the metallic moulds employed [82], alternatively the gap formation is often assumed to be less effective in the cases of sand and investment casting due to the poor conductivity of the sand or ceramic moulds employed [27].

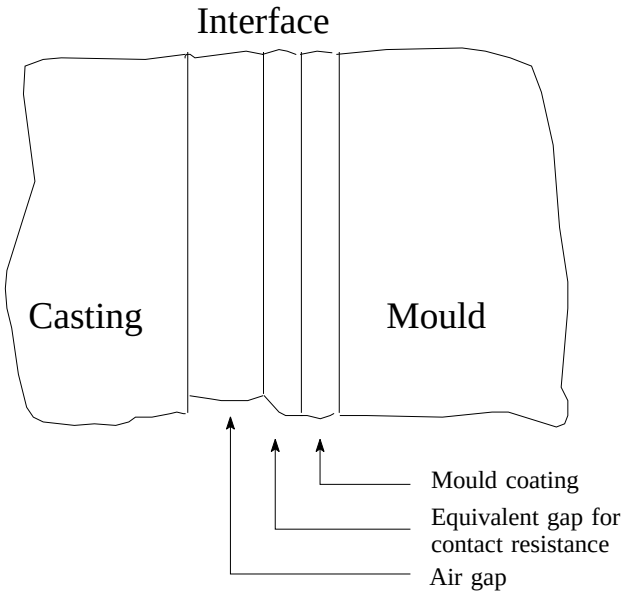

Figure 7.1: The die casting/mould interface.

Considering die casting, the heat transfer coefficient is often assumed to consist of a number of different layers, this leads to a series of thermal resistances as illustrated in Figure 7.1 [82]. In this research the coating layer of the mould is included in the contact resistance and the heat transfer coefficient across the interface h_{if} can be expressed as [82]

$$\frac{1}{h_{if}} = \frac{1}{h_{cr}} + \frac{1}{h_{ag}}, \tag{7.1}$$

where h_{cr} is the heat transfer coefficient of the contact resistance and h_{ag} is the heat transfer

coefficient of the air gap.

The thermal contact resistance $\frac{1}{h_{cr}}$ is caused by the rugosity of the mould, which can cause a non-uniform thermal contact between the melt and the mould [82, 29]. In PHYSICA the die casting/mould interface can be implemented by defining the lower limit of the heat transfer coefficient across the casting/mould interface to be equal to h_{cr}. Consequently, if no air gap exists this value will be assigned to the heat transfer coefficient.

The gap formation in PHYSICA is achieved via coincident nodes at the casting/mould interface, consequently the cell faces at the casting/mould interface are initially coincident [42]. The heat transfer flux is calculated at the respective centres of the initially coincident cell faces and as the gap develops it is computed as the distance between the associated face centres. This is a reasonable method for problems involving small strains as the face associations of the original geometry are not drastically altered due to the mechanical deformation.

As described in Figure 7.1 an equivalent gap Δ_{eq} can be associated with the thermal contact resistance [82]

$$\frac{1}{h_{cr}} = \frac{\Delta_{eq}}{k_{cr}}, \tag{7.2}$$

where k_{cr} is the thermal conductivity associated with the die casting/mould interface, initially.

The complete behaviour of the die casting/mould interface can be implemented using a convective heat transfer flux [63]

$$\frac{\partial T}{\partial n} = h_{\mathit{eff}} \left(T_{casting} - T_{mould} \right), \tag{7.3}$$

where the effective heat transfer coefficient at the casting/mould interface is a function of the effective air gap Δ_{ag} and can be calculated as follows [82, 68];

$$h_{\mathit{eff}} = \begin{cases} h_{cr}, & \text{when } \Delta_{ag} \leq \Delta_{eq} \\ \frac{k_{ag}}{\Delta_{ag}}, & \text{when } \Delta_{ag} > \Delta_{eq} \end{cases}, \tag{7.4}$$

where k_{ag} is the conductivity associated with the air gap.

It is important to note that the gap may not be purely air, a mixture of gases could be possible. Additionally, the heat transfer across the casting/mould interface is not neces-

sarily a solely conductive process. Consequently, an effective conductivity associated with air gap can be utilised to facilitate this behaviour. This requires accurate experimental measurement of the heat transfer coefficient as a function of the gap at the casting/mould interface [82, 12].

7.2 Gravity die casting of a hollow aluminium cylinder

The experimental results, against which the numerical analyses of the die casting of a hollow aluminium cylinder are compared, were originally obtained by Schmidt and Svensson [82]. They experimentally studied the heat transfer and air gap formation associated with the die casting of aluminium alloys. A large number of experiments were performed, under a variety of casting conditions and with a selection of aluminium alloys.

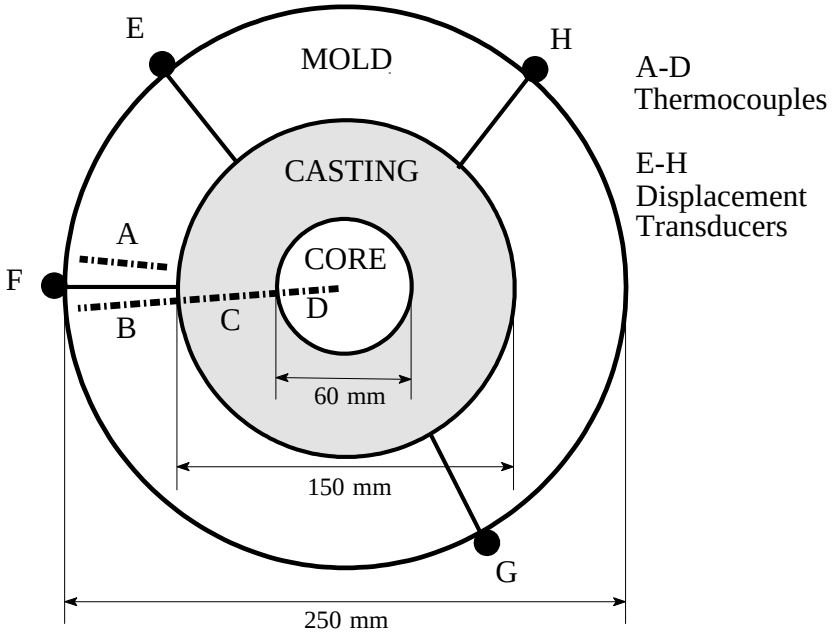

Figure 7.2: Experimental design: Top view.

The particular experimental design, with regard to geometry, thermocouples and displacement transducers, that was employed to obtain the experimental data utilised in this re-

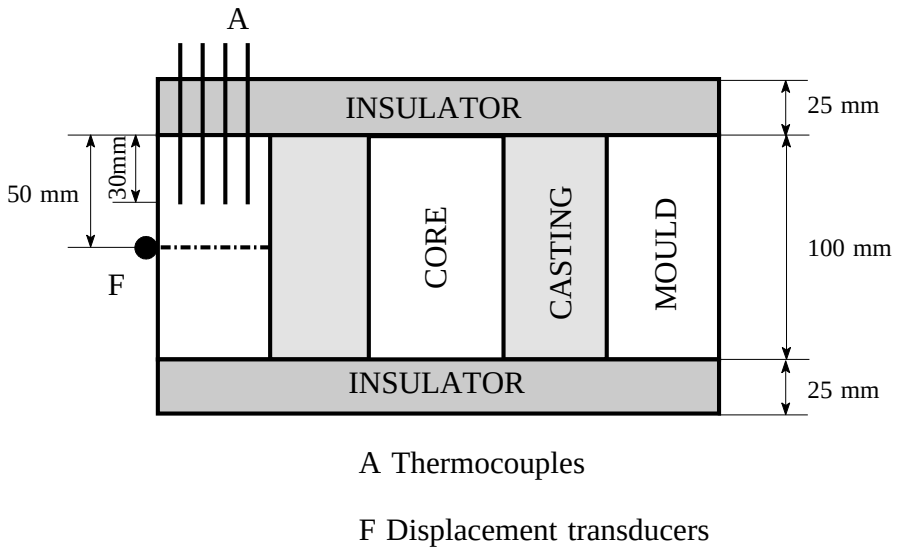

Figure 7.3: Experimental design: Side view.

search, is illustrated in Figures 7.2 and 7.3.

It is important to note the positioning of, both, the thermocouples and the displacement transducers. The thermocouples are arranged along the radius of the die casting design, as illustrated in Figure 7.2, to enable inverse heat transfer analyses to be performed at a variety of time intervals. Additionally, a number of displacement transducers are located at mid-height with regard to the aluminium casting, as illustrated in Figure 7.3. Which furnishes an average measurement of the gap formation at the mid-height point over time.

The cylindrical mould and core are made of steel (Fe–0.14%C–0.35%Si–1.2%Mn) and the cylindrical casting consists of the aluminium alloy (Al–7%Si–0.3%Mg). The associated material properties are described in Tables 7.3 and 7.2, respectively. As illustrated in Figures 7.2 and 7.3 the experimental design is axisymmetric and, after the filling of the mould, the top and bottom of the mould are insulated. In this manner, the majority of the heat transfer associated with the cooling and subsequent solidification of the casting is confined to the radial direction.

Heat transfer coefficient ($W/(m^2K)$)	400	20.0
Gap distance (mm)	0	0.5

Table 7.1: Relationship between heat transfer coefficient and gap distance.

From the experimental results and the, consequential, inverse heat transfer analyses, it is possible to obtain a relationship between the heat transfer coefficient at the gap and the gap size [82]. In this research the experimentally obtained relationship was suitably approximated by a linear relationship as described in Table 7.1. The values associated with the heat transfer coefficient are particularly low in this experimental case due to the extra thermal resistance of the coating layer. Indeed, for experimental the cases not involving a coating layer the heat transfer coefficient values are an order of magnitude greater [82].

7.2.1 Numerical analysis

The die casting experiment described here, has been previously modelled in three dimensions, by Bellet et al [12, 67, 13], utilising the FEM. As a complex, three dimensional, fully coupled, thermo-mechanical numerical analysis, the experimental casting provides a comprehensive validation test with regard to the FV software framework PHYSICA.

With regard to the thermal analysis the following assumptions were made. After pouring the liquid aluminium alloy is assumed to be static and residual convection is neglected. The liquid alloy is assumed to be at an initial, uniform, temperature of 800°C, the mould, core and insulation are at a, pre-heated, uniform temperature of 200°C and the insulators are at an initial, uniform, temperature of 20°C. These initial temperatures are consistent with the experimental analysis [82].

For the solidification, the latent heat of fusion is assumed to be constant during the solidification phase, hence simplifying the solidification analysis. The numerical methods employed in the thermo-mechanical test case involving solidification, which was described in the previous Chapter, are employed again. It should be noted that it is possible to model the solidification phase with greater accuracy, by accounting for the eutectic behaviour associ-

ated with a binary alloy [12, 82]. This method involves the latent heat of fusion as a function of temperature, but as yet this facility is not implemented within PHYSICA. Fortunately, this loss of accuracy is acceptable with regard to the modelling of the gap formation at the casting/mould interface and associated heat transfer. The material properties associated with the thermal analysis are described in Tables 7.2, 7.3 and 7.4, the additional material properties required for the solidification analysis of the aluminium alloy are highlighted in Table 7.2.

T_L	Liquidus temperature		618.8°C
T_S	Solidus temperature		566.4°C
h	Latent heat of fusion		440 kJ/kg
k	Thermal conductivity		150 W/(mK)
ρ	Density		2,710 kg/m^3
c	Specific heat capacity		1160 J/(kgK)
α	Coefficient of thermal expansion		5×10^{-5} /K
ν	Poisson's ratio		0.33
E	Young's modulus	60,000MPa	20°C
		34,000MPa	450°C
		1×10^{-2}MPa	566.4°C
Y	Yield stress	500MPa	20°C
		1×10^{-4}MPa	566.4°C

Table 7.2: Material properties of the aluminium casting alloy.

With regard to the boundary conditions at the external faces of the mould and insulators, as illustrated in Figures 7.4(2) and (4), a convective cooling condition is assumed, with a heat transfer coefficient of 20W/(m^{2}K) and an ambient temperature of 20°C, between these faces and the surrounding air. At the internal faces, when the casting is in contact with the mould, a heat transfer coefficient of 400W/(m^{2}K) is assigned. When a gap occurs between the casting and the mould, the experimentally obtained relationship between the gap distance and the heat transfer coefficient is employed. Additionally, symmetry planes are assigned with regard to the heat transfer in the x and z directions, as illustrated in Figures 7.4(1), (2), (3) and (4).

With regard to the mechanical analysis the following assumptions were made. The mould, core and insulators as described in Figures 7.2 and 7.3 are assumed to be rigid and their

k	Thermal conductivity	33 W/(mK)
ρ	Density	7,880 kg/m^3
c	Specific heat capacity	600 J/(kgK)

Table 7.3: Material properties of the mould and core steel.

k	Thermal conductivity	0.1 W/(mK)
ρ	Density	1,000 kg/m^3
c	Specific heat capacity	1,760 J/(kgK)

Table 7.4: Material properties of the insulation.

dilation due to heating is neglected.

The contact between the casting and the core, insulators and mould is accounted for by applying fixed displacements of zero to the casting a priori. The simple geometry of the casting allows this approach to be performed easily. As the casting cools and solidifies it will contract around the, assumed rigid, core. Hence, the x and z displacements are fixed to zero at the nodes on the inner face of the casting, as illustrated in Figures 7.4(2) and (3). Additionally, due to gravity the base of the casting will rest on the, assumed rigid, base insulator. Hence, the y displacement components are fixed to zero at the nodes on the base of the casting as illustrated in Figures 7.4(3) and (4). The x and z displacement components are set to zero at the nodes on the respective symmetry planes as illustrated in Figures 7.4(1) and (3). The material properties associated with the mechanical analysis are highlighted in Table 7.2. Obviously, no mechanical material properties are required for the mould, core and insulation as they are assumed to be rigid.

The thermal and mechanical material properties, as described in Tables 7.2, 7.3 and 7.4, were obtained from a number of sources, including the original experimental analysis [82, 12, 67, 87]. The thermal expansion coefficient has been suitably modified to account for shrinkage during the phase change.

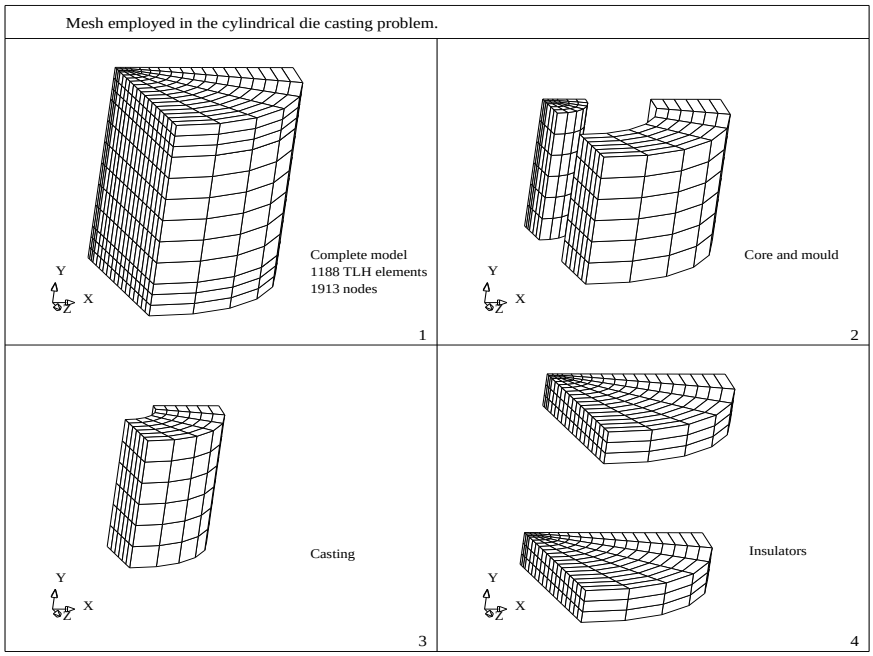

Figure 7.4: Mesh employed in the analysis of gravity die casting.

7.2.2 Discussion of numerical results

The die casting problem described here, was originally proposed by Bellet et al [13, 67, 12] as evidence for the necessity of a coupled thermo-mechanical treatment in the modelling of the die casting process.

This was achieved by first performing a purely thermal analysis and neglecting the mechanical analysis. In this manner, the heat transfer coefficient is initially assumed constant at the casting/mould interface. Secondly, a thermo-mechanical analysis is performed and the heat transfer coefficients at the casting/mould interface can vary as a function of the gap formed there. These analyses were performed in the FV framework PHYSICA and the results are illustrated in Figures 7.5, 7.7, 7.12 and 7.13. The contraction of the cylindrical casting and the resultant gap formation over time is illustrated in Figure 7.7. The radial stresses, hoop stresses and hoop visco-plastic strains associated with the temperature fields at 500 and 900 seconds, are illustrated in Figures 7.12 and 7.13, respectively.

The temperature profiles over time are plotted at points approximately 5mm from the casting/mould interface, with regard to both the casting and the mould. The temperature profile in the casting is initially at 800°C, when the casting is completely liquid. The casting then cools to the liquidus temperature in a linear fashion, at which time solidification begins. The casting then cools again in a linear fashion until the solidus temperature is reached. During these initial stages of cooling the thermal and thermo-mechanical analyses are in agreement. It is at solidus and sub-solidus temperature that the cooling rates vary and it is during this stage that the thermo-mechanical analysis is closer to the experimental results. Indeed, at 900 seconds the thermal analysis differs by approximately -50°C with regard to the thermo-mechanical and experimental results.

Similar, but not as drastic behaviour is also illustrated by the temperature profile in the mould, which heats quickly from the initial temperature of 200°C before solidification begins and then levels out. The gap formation at the casting/mould interface is illustrated in

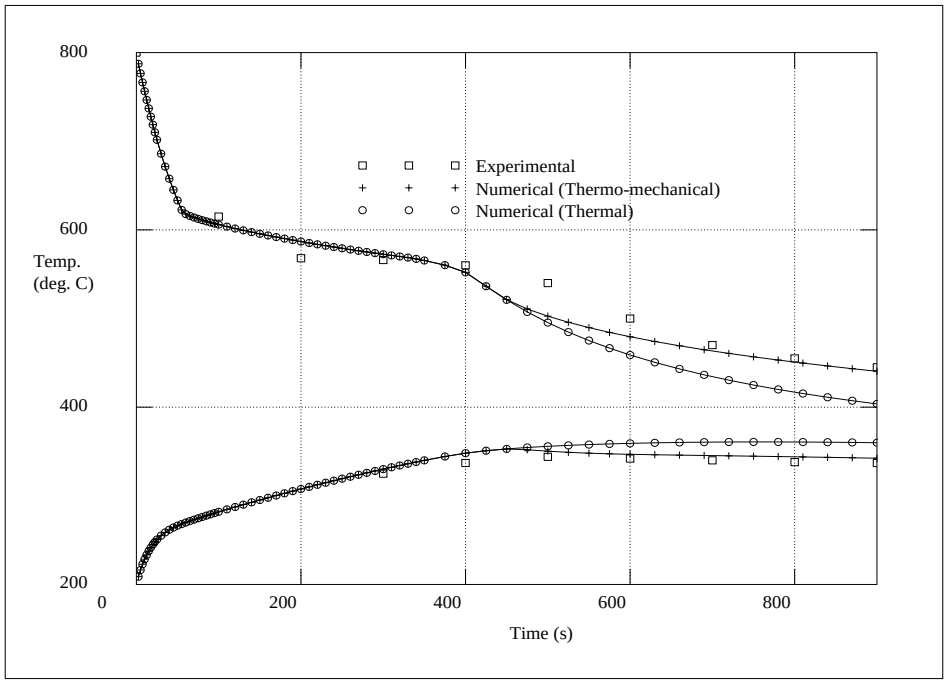

Figure 7.5: Temperature profiles in mould and casting.

Figure 7.6 and is in good qualitative agreement with the experimental results. The gap prediction could be quantitatively improved if, either a more accurate solidification analysis

was performed, as discussed in the previous section, which would furnish a longer freezing range [82] and hence later gap formation, or the mould and core dilation was included in the mechanical analysis which could enlarge the gap size.

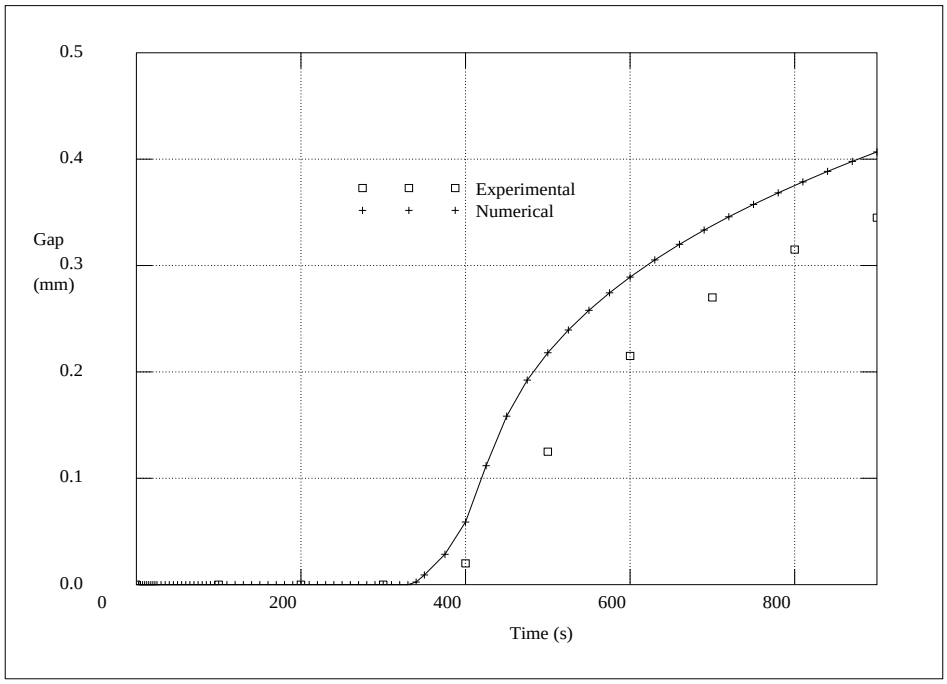

Figure 7.6: Gap formation at mould/cast interface.

Initially, the analysis was performed assuming rate independent elasto-plastic behaviour and the results were illustrated in Figures 7.5 and 7.6. Secondly, the analysis was performed assuming rate dependent elasto-visco-plastic behaviour. This was achieved by employing the additional material properties as described in Table 7.5 [13, 67, 12], and in this analysis the time interval associated with the mechanical analysis must not exceed that employed during the thermal analysis. The results are compared against those of the rate independent

		20°C	566.4°C
γ	Fluidity (/s)	1.0×10^6	3.7×10^3
m	Rate sensitivity	0.02	0.2

Table 7.5: Rate dependent material properties.

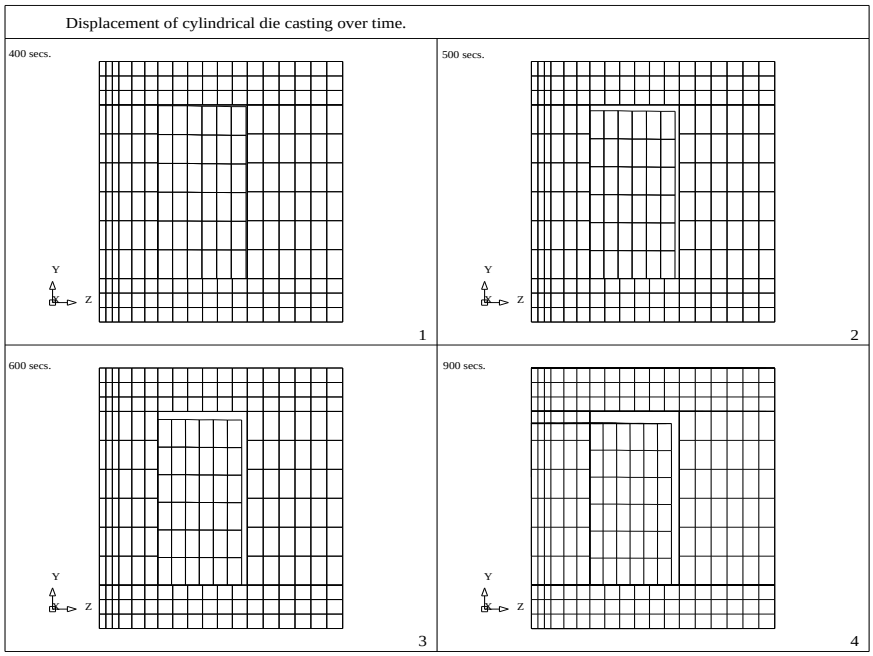

Figure 7.7: Casting shrinkage and gap formation over time (Mg. ×10).

analysis in Figures 7.8 and 7.9. Surprisingly, the two analyses are in remarkably close agreement. This may be attributable to the insensitivity of the algorithmic approach, as described in this research, to rate dependent material non-linearity over the sub-solidus temperature range or to the possibility that viscous effects are negligible when the cooling rates are are extreme, such as those exhibited in die casting. The latter hypothesis is reinforced by the negligible viscous effects exhibited in quenching problems as discussed in the previous chapter. These points are of considerable interest and may well point to further avenues of research.

When considering the possibility of residual convection of the liquid metal in the casting after pouring, it is informative to study the temperature profiles at the inner and outer surfaces of the cylindrical casting and, additionally, at a point in the centre of the casting. These profiles are illustrated in Figure 7.10. Obviously, with regard to the liquid phase, negligible thermal gradients exist and hence no buoyancy driven recirculation will occur. The slight thermal gradients appearing during the solidification phase will be ineffective due to the permeability coefficient appearing in the momentum equations when solidification is

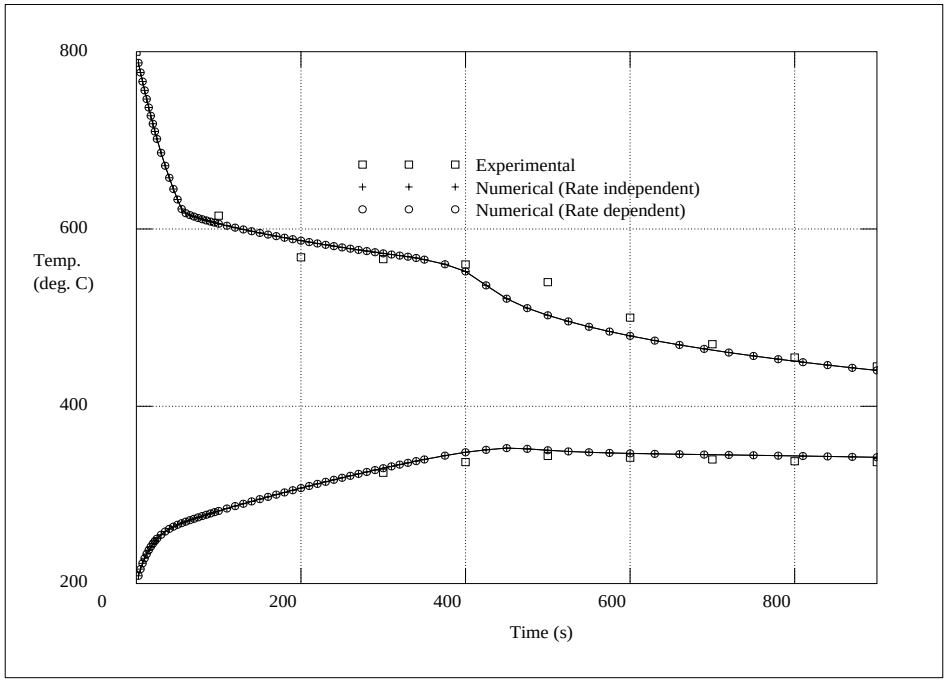

Figure 7.8: Temperature profiles in mould and casting.

occurring.

At present further contributions to residual convection due to the material dilation during phase changes and porosity formation are not available within the PHYSICA framework. Though it should be noted that research is underway to extend the two dimensional treatment of Fryer et al [42, 3] for inclusion within the PHYSICA framework. The heat transfer problem involving solidification as associated with the die casting problem described here, was simulated with and without the inclusion of convection. With regard to the analysis including convection a constant viscosity was employed $\mu = 2.0 \times 10^{-3}\mathrm{Ns/m}^2$. Wall boundary conditions were applied at the casting/mould and casting/insulator interface, which furnished the required momentum boundary conditions.

As illustrated in Figure 7.11 the inclusion of convection due to buoyancy driven recirculation has no observable effect on the heat transfer. Indeed, this is consistent with the design of the experimental analysis which is intended to restrict heat transfer to conduction only.

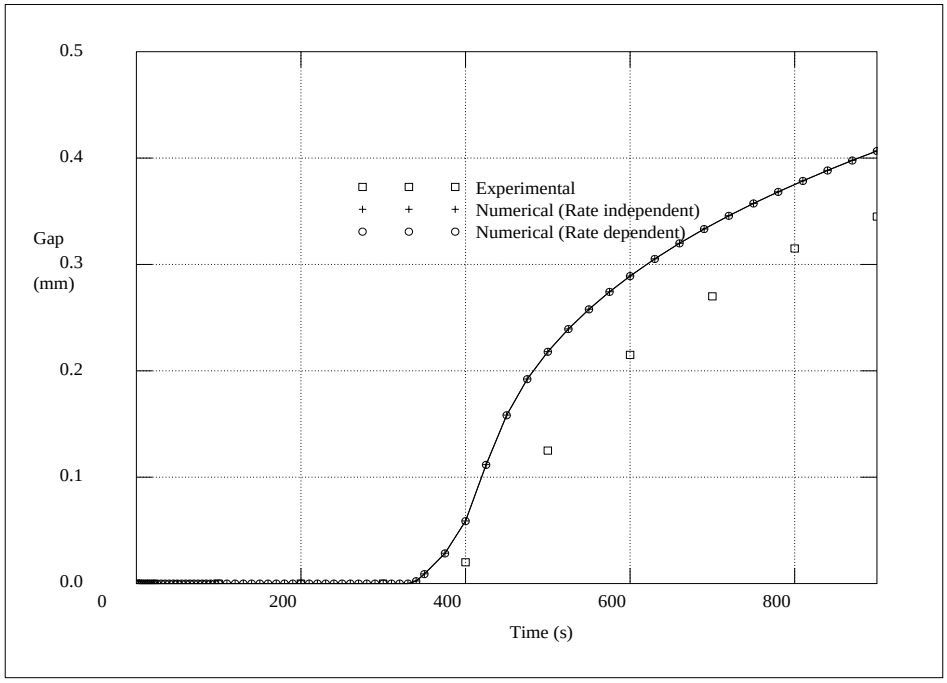

Figure 7.9: Gap formation at mould/cast interface.

In order to assess the accuracy and stability of the thermo-mechanical coupling technique employed in this research, a number of analyses were performed with different time intervals relating to the thermal and mechanical staggering. The results obtained are illustrated in Figures 7.14 and 7.15. With regard to scheme 1 an increasing time interval was employed, which ranged from a value of 2.5 to 30 seconds, this scheme is the most accurate and was employed generally. With regard to schemes 2 and 3 a fixed time interval of 30 and 60 seconds was employed, respectively. It should be noted that employing a greater time interval reduces the accuracy of the solidification analysis, and the outcome can be misleading as the resultant cooling rate and gap formation appear closer to the experimental results.

Additionally, in order to investigate mesh dependency, the mesh was refined by increasing the number of divisions in the radial direction. Initially, a fine mesh consisting of 2,112 elements and 3,201 nodes and finally a coarser mesh consisting of 1,118 elements and 1913 nodes was employed. As illustrated by Figures 7.16 and 7.17 the results are reasonably mesh independent.

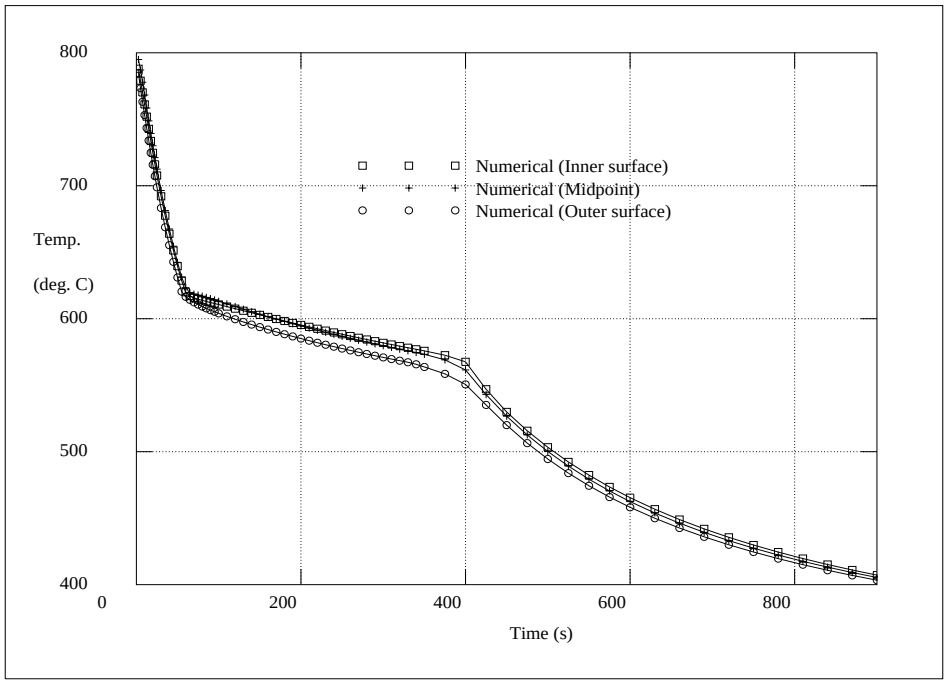

Figure 7.10: Temperature profiles in the casting.

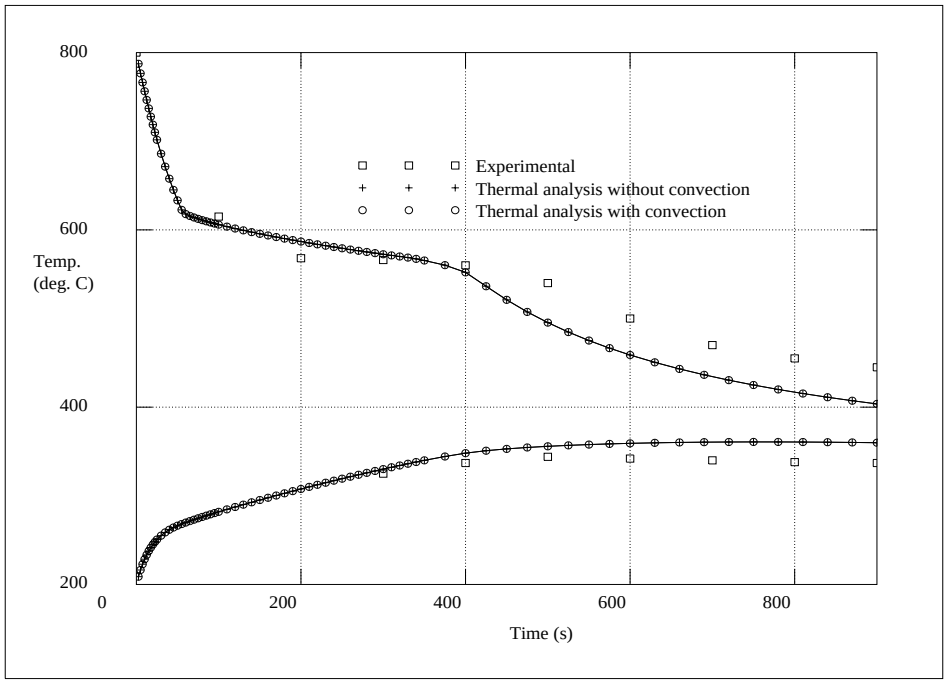

Figure 7.11: Temperature profiles in mould and casting .

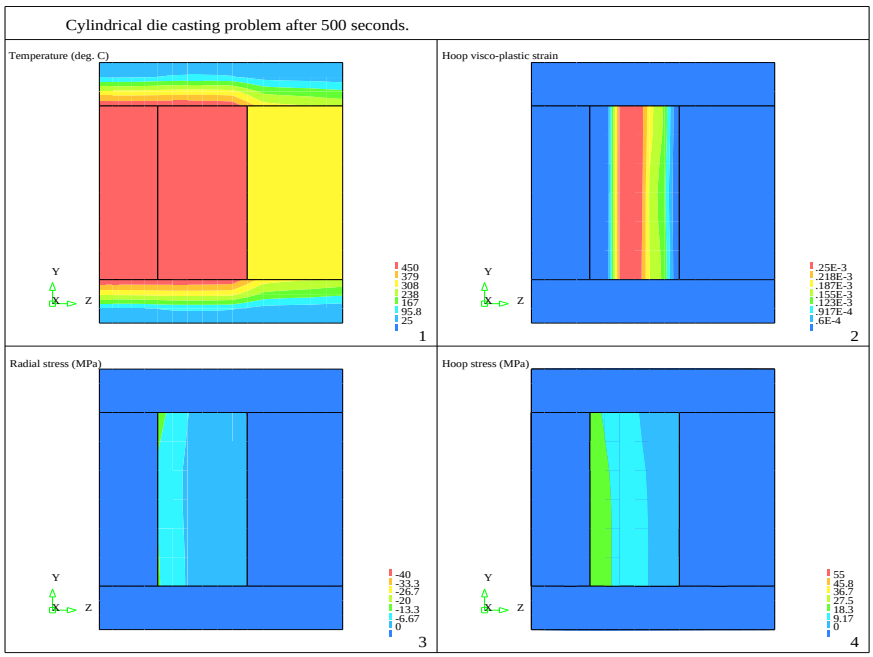

Figure 7.12: Stress and visco-plastic strain at 500 seconds.

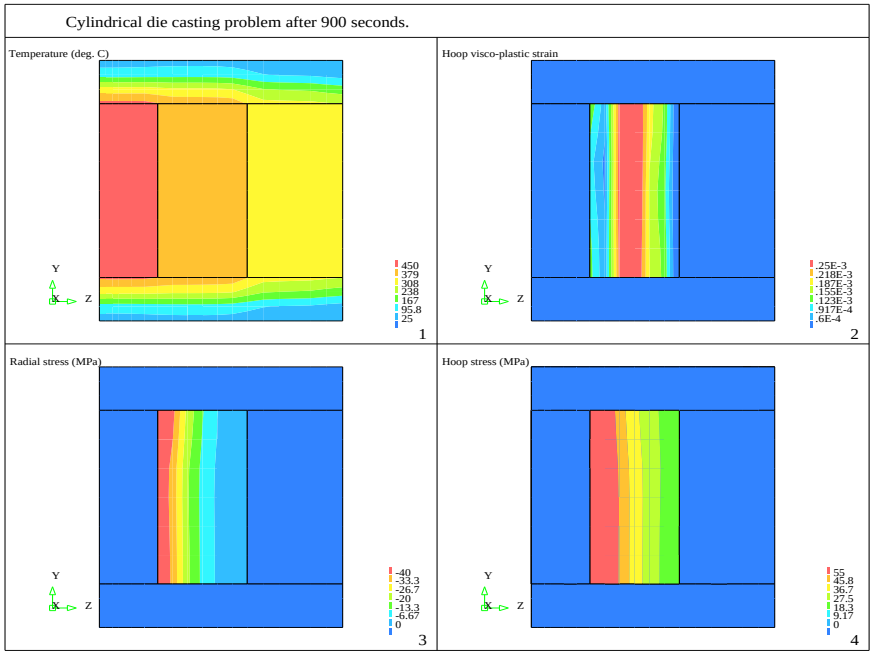

Figure 7.13: Stress and visco-plastic strain at 900 seconds.

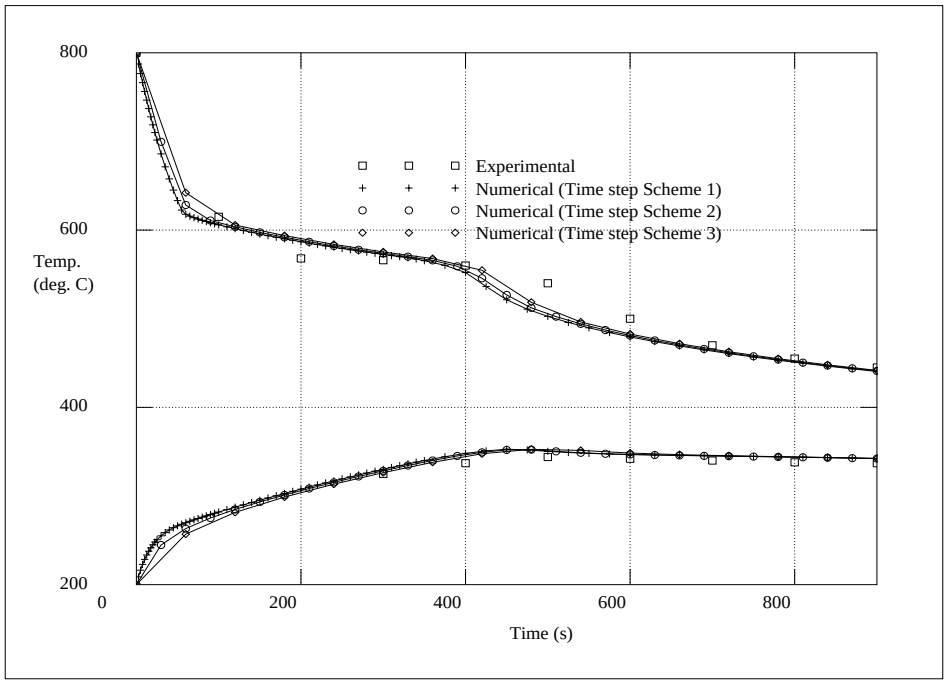

Figure 7.14: Temperature profiles in mould and casting .

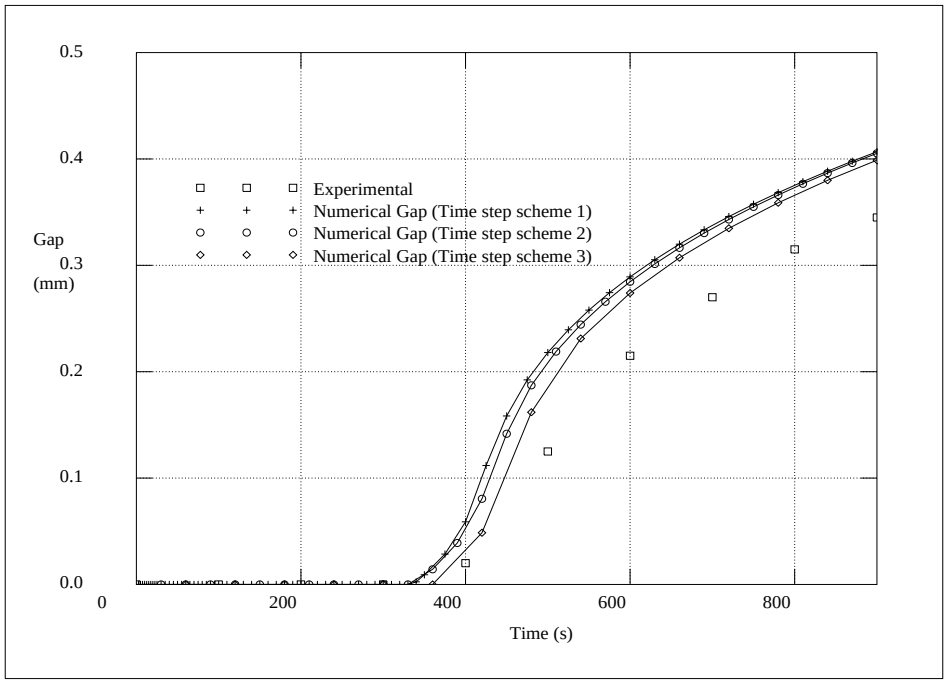

Figure 7.15: Gap formation.

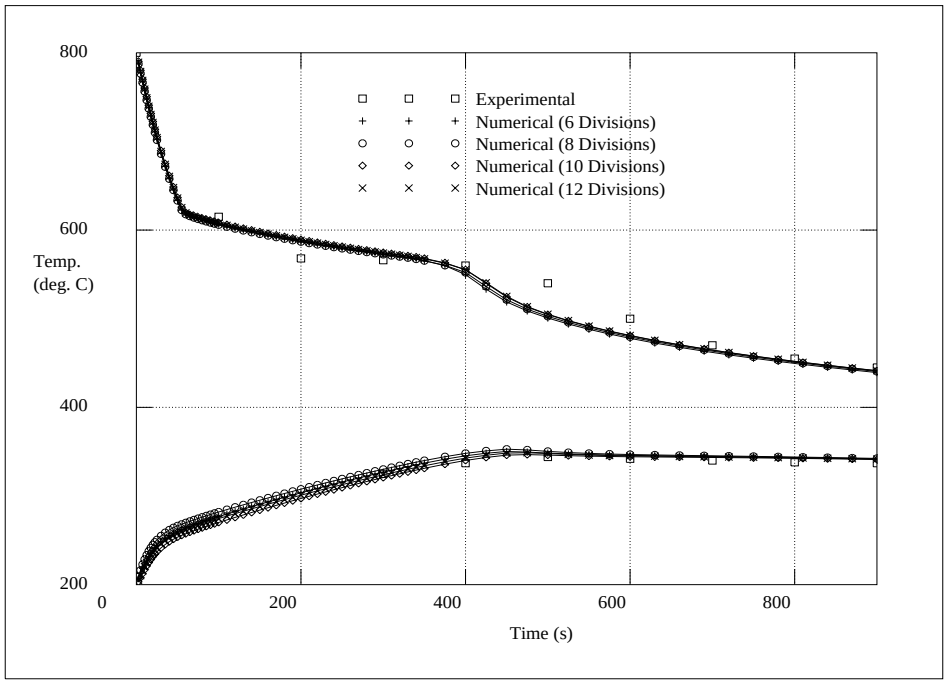

Figure 7.16: Temperature profiles in mould and casting .

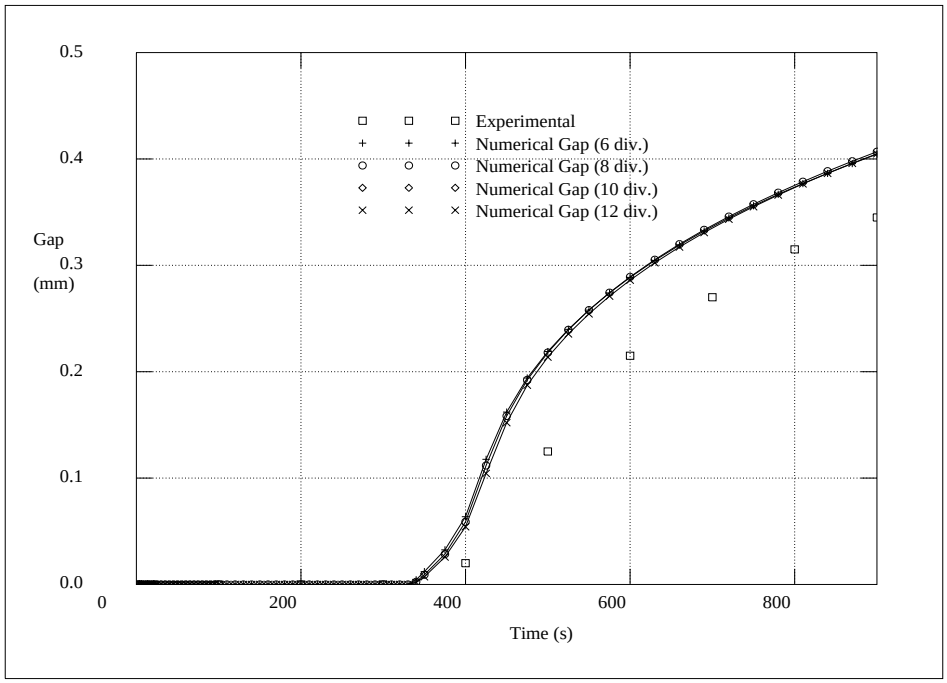

Figure 7.17: Gap formation.

7.3 Sand casting of an aluminium test bar

The experimental analyses of the sand casting of aluminium test bars were originally performed by Castings Technology International (CTI) and modelled by Chow et al [21] with material property data originally provided by the National Physics Laboratory [21].

The objective of these experimental investigations was to observe porosity formation as associated with shrinkage defects [21]. Unfortunately, to the best of the authors knowledge, no thermal or mechanical results were recorded during these experiments. However, with regard to the simulation of the shape casting of metals, the test bar problem as illustrated in Figures 7.18, 7.19, 7.20 and 7.21 provides a suitable academic illustration of the present capabilities and future requirements of the engineering software PHYSICA.

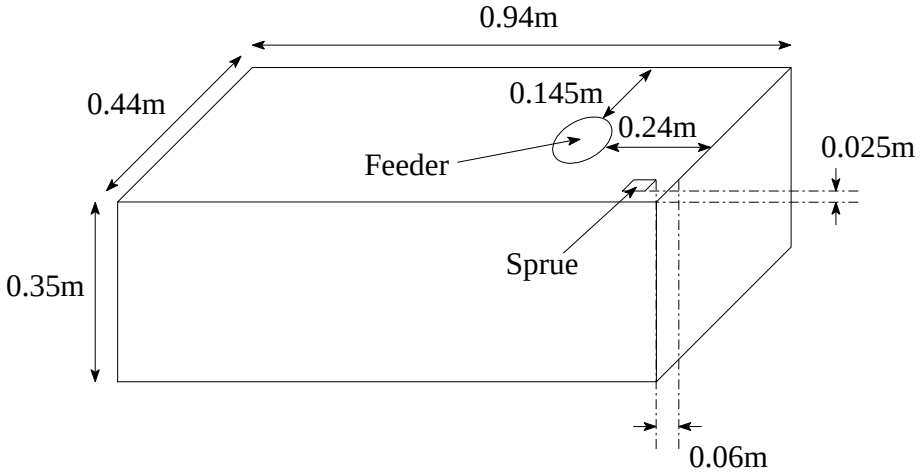

Figure 7.18: Geometry of the sand mould.

In these experiments a 10mm thick insulation sleeve was placed around the feeder, as illustrated in Figure 7.22(4), and the moulds consisted of chemically bonded sand.

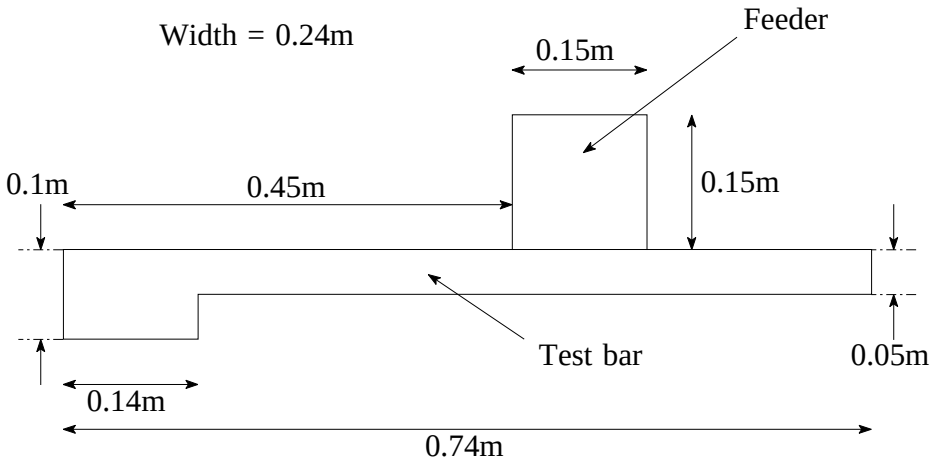

Figure 7.19: Geometry of aluminium test bar (without sprue).

7.3.1 Numerical analysis

With regard to the thermal analysis the liquid metal alloy is assumed to be static initially and at a uniform temperature of 714°C, alternatively the mould and insulation sleeve are at a uniform temperature of 25°C. These initial temperatures are consistent with experimental analysis [21].

The chemically bonded sand and the insulation sleeve have thermal conductivities of 0.8 W/(mK) and 0.39 W/(mK), respectively. The heat transfer coefficient applied at the casting/mould interface when the mould and cast are in thermal contact is 1500 W/(m^2K). This value is higher than that employed in the die casting problem, where a coating layer applied at the casting/mould interface increased the thermal resistance. Additionally, the heat transfer coefficient at the casting/mould interface is assumed to vary linearly with the gap formation, the conductivity of the gap is equivalent to that described for the die casting problem in Table 7.1. The aluminium alloy employed in the sand castings is assumed

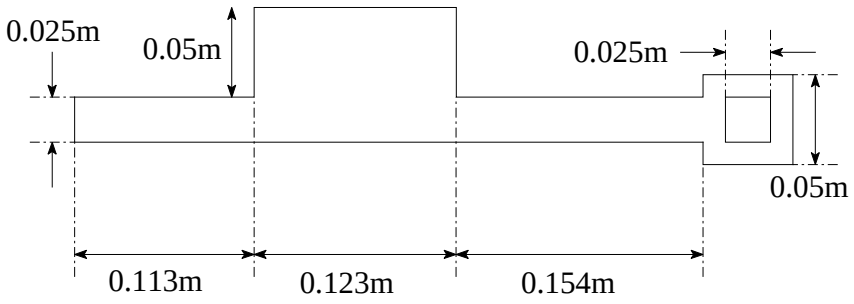

Figure 7.20: Geometry of sprue (top view).

equivalent to that of the previous die casting problem and the material properties are those described in Tables 7.2 and 7.5.

Considering the solidification, the same assumptions were applied as in the die casting problem. With regard to the thermal boundary conditions, a convective cooling condition with a heat transfer coefficient of 1000 W/(m^{2}K) and an ambient temperature of 25°C is applied at all the external surfaces except the feeder surface which is assumed to be adiabatic. Hence, it is ensured that the alloy remains liquid in the feeder longer than anywhere else in the test bar.

With regard to the mechanical analysis the following assumptions were made. The thermal contraction of the test bar is constrained by the mould geometry and gravitational effects. As in the die casting problem, the mould is assumed to be rigid and the contact constraints are applied a priori. Unfortunately, as illustrated by the geometry of the casting in Figure 7.22(3), it is no longer immediately obvious where the mechanical constraints should be applied a priori. In this case a number of mechanical constraints have been applied, which

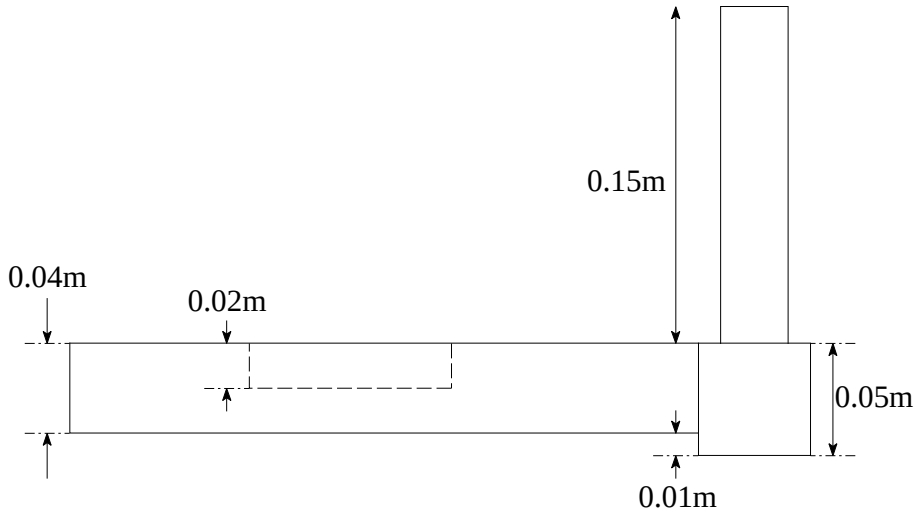

Figure 7.21: Geometry of sprue (side view).

can be assumed to satisfy contact conditions between the mould and casting. However, it is important to note that even for such a simple geometry as this test bar, once the sprue and feeder are included, as illustrated in Figure 7.22(3), a more physically accurate contact algorithm is preferable. Indeed, present research is underway to include a completely coupled deformable-deformable FV contact algorithm within the PHYSICA framework.

7.3.2 Natural convection

Considering the heat transfer associated with this problem it is appropriate to investigate the effects of buoyancy driven recirculation. This is attributable to the problem geometry, which furnishes the necessary thermal gradients during the cooling of the liquid alloy.

However, for this problem it is interesting to compare heat transfer by conduction and convection with heat transfer by conduction only. It should be noted that any natural convection which occurs can contribute to the heat transfer and will modify the thermo-

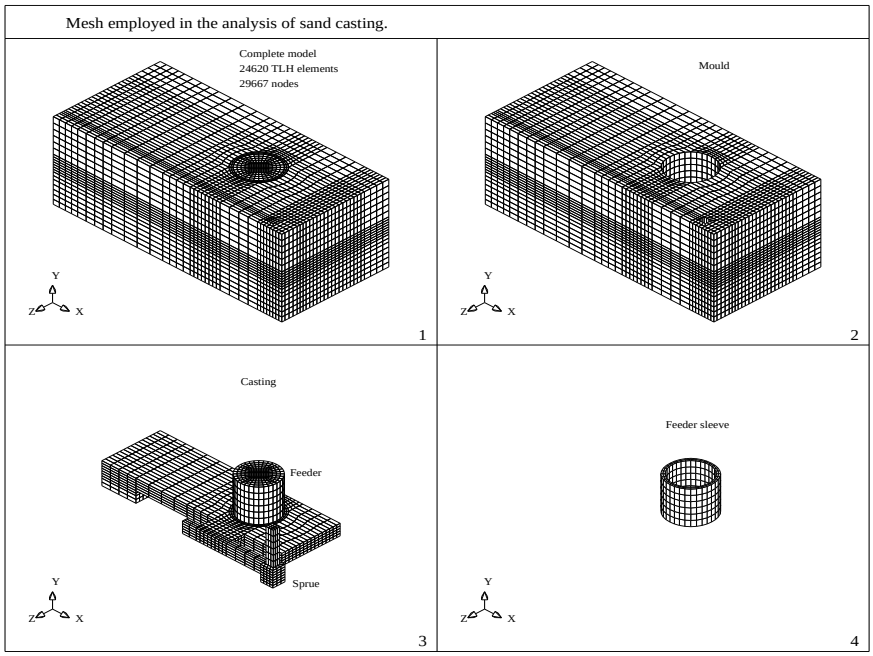

Figure 7.22: Mesh employed in the analyses of the CTI test bar.

mechanical behaviour of the casting and mould. Additionally, the quality and soundness of the casting can be affected by other resulting transport phenomena, such as the convection of solute produced by alloy segregation, which can significantly affect the solidification of the alloy [16]. At present this capability is not available within the PHYSICA framework, but current research is underway to facilitate this capability also.

The buoyancy driven recirculation is furnished by employing the Boussinesq approximation. Where the viscosity is assumed to have a constant value of 1.3×10^{-3}Pas, the flow is assumed to be laminar and wall friction boundary conditions are applied at the casting/mould interface.

7.3.3 Discussion of numerical numerical results

In this section the numerical results of the sand casting problem will be discussed. Initially, the results of the thermal analyses that were performed will be discussed and finally the

results of the thermo-mechanical analyses that were performed will be discussed.

7.3.3.1 Thermal analyses

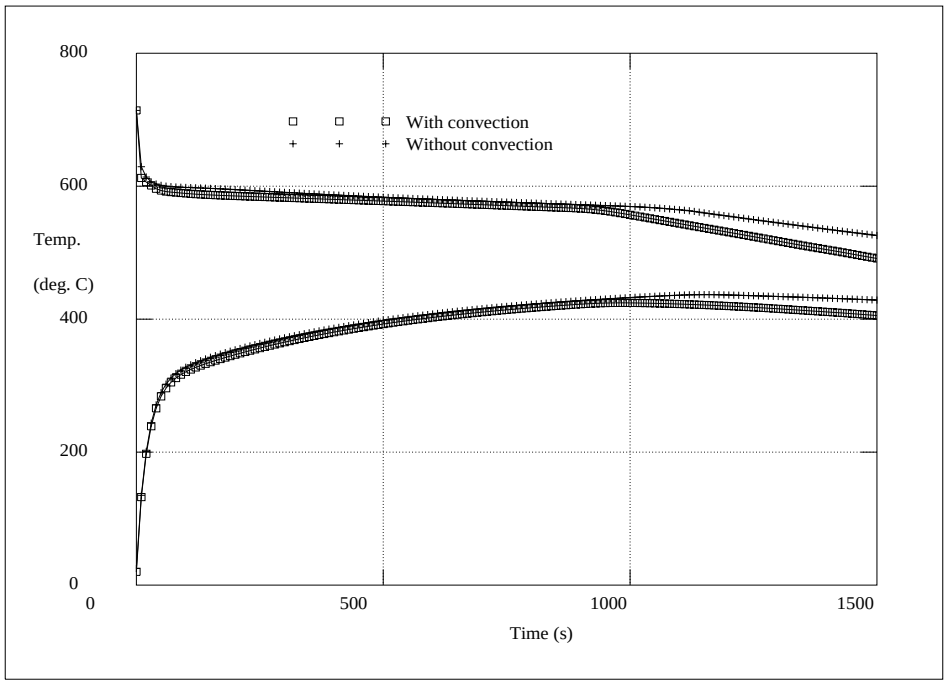

Figure 7.23: Cooling rates in the test bar and sand mould.

Initially, several thermal analyses of the sand casting problem were performed and the associated mechanical behaviour was neglected. In the thermal analyses the casting was considered for problems with and without convection. In this manner, it was possible to investigate the effects of the inclusion of natural convection in the sand casting simulation.

In both cases the thermal analyses were simulated for 1500 seconds, at which time the test bar had completely solidified. With regard to the computational effort, the analyses required 15 to 20 hours CPU time on a SPARC 20 100 MHz work station with 320 Mbytes of main memory. The thermal analysis including natural convection required approximately 25% additional CPU time.

The cooling rates at points 5cm either side of the centre of the base of the casting/mould

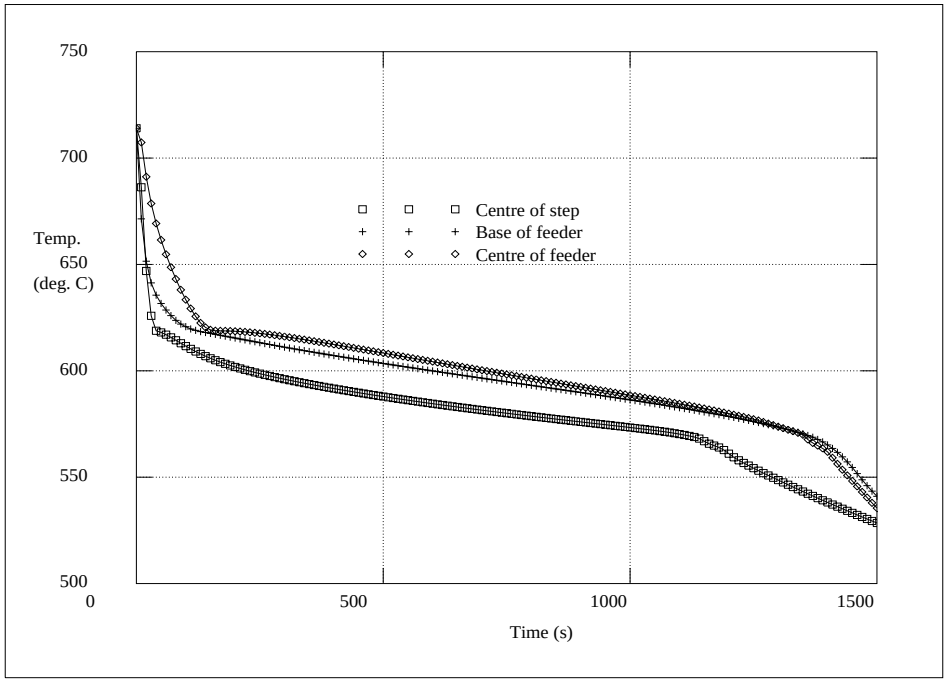

Figure 7.24: Cooling rates for heat transfer without convection (1500 secs.).

interface are illustrated in Figure 7.23. Additionally, the cooling rates at several positions within the test bar are illustrated in Figures 7.24 and 7.25 for the thermal analyses, with and without natural convection respectively.

With regard to the simulation that included natural convection it should be noted that the temperatures are approximately 20°C to 30°C cooler in the casting and the mould after 1500 seconds. This can be attributed to the mixing effect of the natural convection, which will redistribute the temperatures in the casting more evenly. Hence, providing greater temperature differences at the casting mould interface which in turn can lead to greater heat transfer at the interface. This phenomenon is more clearly illustrated by considering figures 7.31, 7.32, 7.33 and 7.34.

Considering in more detail the thermal analysis with natural convection included, the recirculations associated with natural convection are clearly illustrated after 20 seconds in Figure 7.35. It should be noted that the present analysis assumes initial uniform temperatures throughout the casting and mould and that the liquid alloy is initially static. This

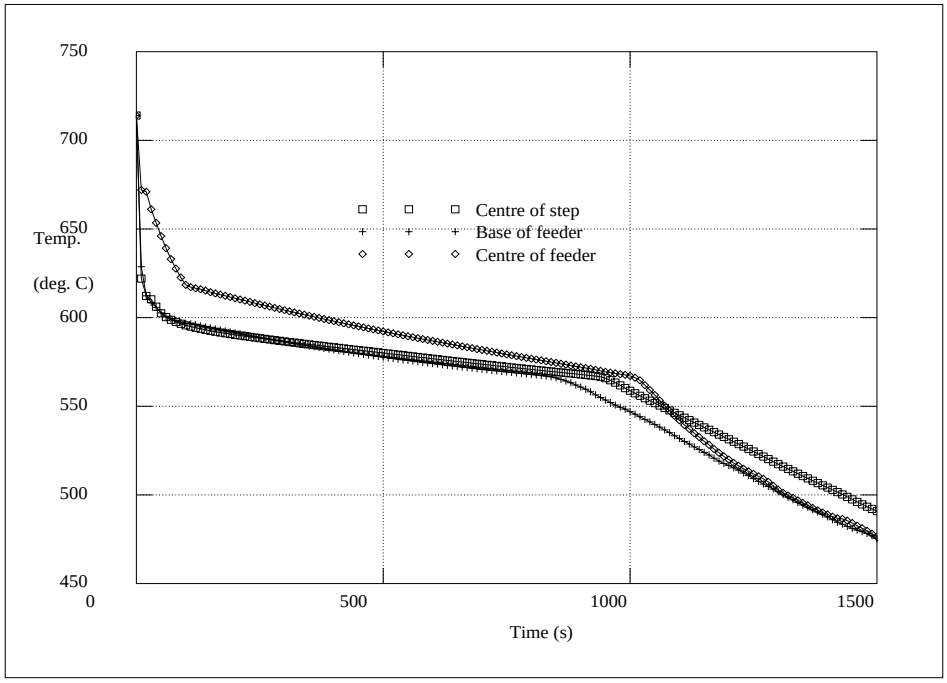

Figure 7.25: Cooling rates for heat transfer with convection (1500 secs.).

neglects any heat transfer that can occur during the filling of the sand mould and any residual flow in the liquid alloy after the filling. Present research is underway to include a filling capability coupled with heat transfer within the PHYSICA framework.

For these reasons the initial flow patterns change quite dramatically and it is interesting to note that a sharp transition occurs in the cooling rate in the feeder during the liquid phase. This phenomenon can be observed in Figure 7.25 and more clearly in Figures 7.27 and 7.28. The phenomenon is obviously not occurring in the thermal analysis without convection as illustrated in Figures 7.24 and 7.26. This phenomenon is attributable to the transition between the reasonably active natural convection which occurs originally and the more sedate natural convection occurring later in the analysis. This is more clearly illustrated by the variation of the velocity and temperature profiles over time, as plotted across the diameter of the feeder in Figures 7.29 and 7.30, respectively. The velocity and temperature profiles are typical of those associated with recirculatory flows and as can be observed the flows subside significantly as the temperature is redistributed more evenly and the heat transfer at the casting/mould interface reduces. Obviously if the mould were pre-heated

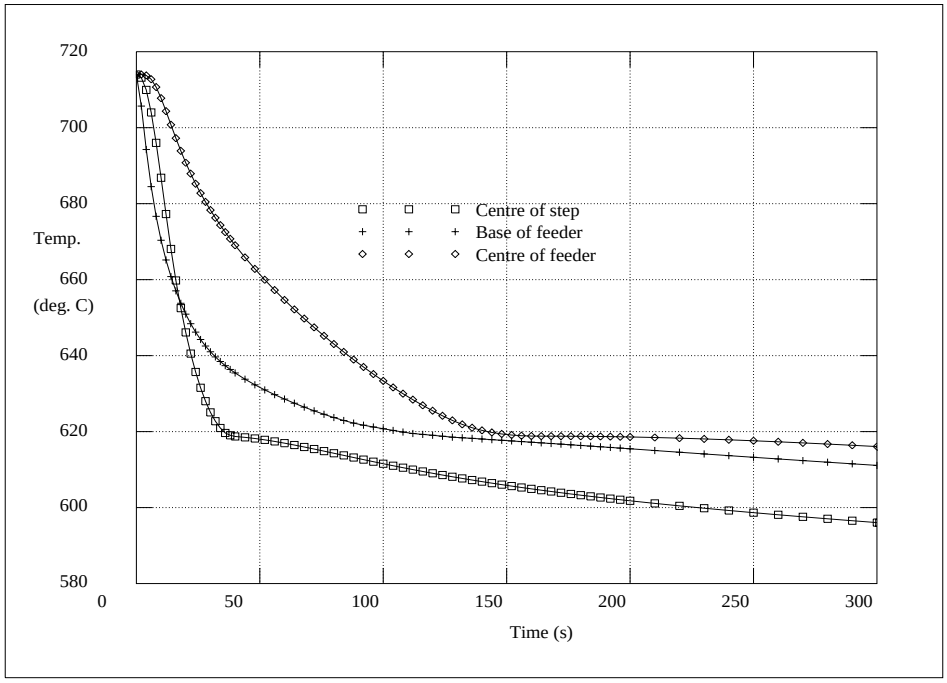

Figure 7.26: Cooling rates for heat transfer without convection (300 secs.).

the effect would be less significant.

Finally, it should be noted that a finer mesh than that illustrated in Figure 7.22 would improve the accuracy of the thermal analysis when including natural convection. Unfortunately, a finer mesh would be prohibitive for a thermo-mechanical analysis with regard to memory requirements and computational effort. For these reasons the mesh described in Figure 7.22 was employed in all the analyses of the sand casting problem.

It should be noted that the inclusion of natural convection in the casting simulation and the consequential effect upon the cooling rates requires further validation and is included in this research as an additional feature presently available within the PHYSICA framework.

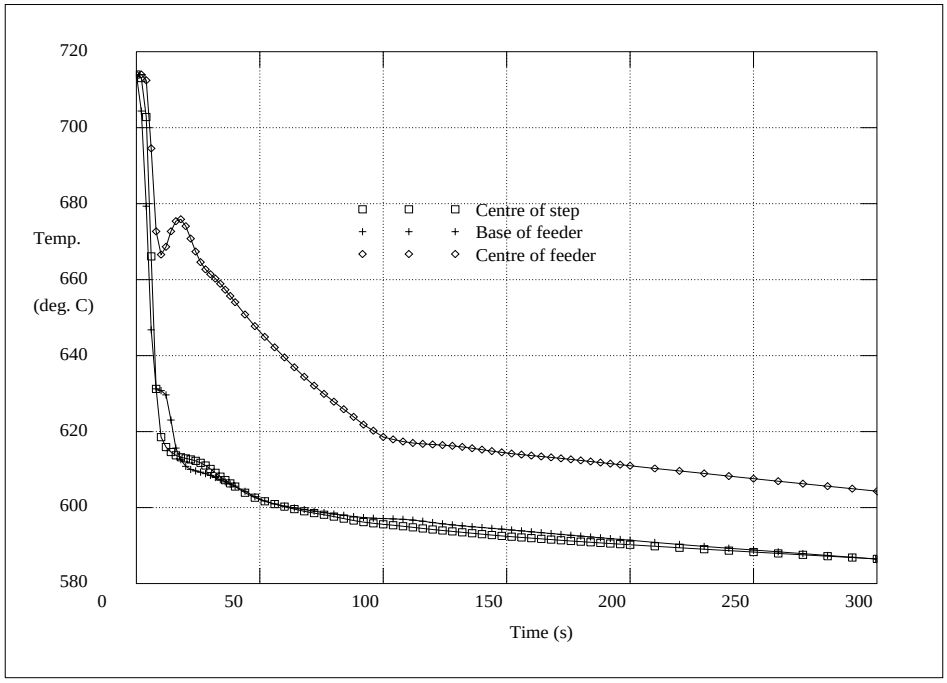

Figure 7.27: Cooling rates for heat transfer with convection (300 secs.).

7.3.3.2 Thermo-mechanical analyses

Several thermo-mechanical analyses were performed with regard to the sand casting problem. Initially, the thermo-mechanical analysis was investigated with and without the inclusion of natural convection and finally the thermo-mechanical analysis was investigated with regard to rate dependent material behavior.

The thermo-mechanical analyses were somewhat limited by memory requirements, which increased by a factor of three for the thermo-mechanical analysis including convection and a factor of five for the thermo-mechanical analysis without. More significantly, the thermo-mechanical analyses were severely limited by the computational effort required. A simulation of 300 seconds required 50 to 60 hours CPU time on a SPARC 20 100 MHz processor with 320 Mbytes main memory.

The deformation of the test bar after 300 seconds is illustrated in Figure 7.36. The deformation has been magnified by a factor of ten and it is obvious that the contact constraints

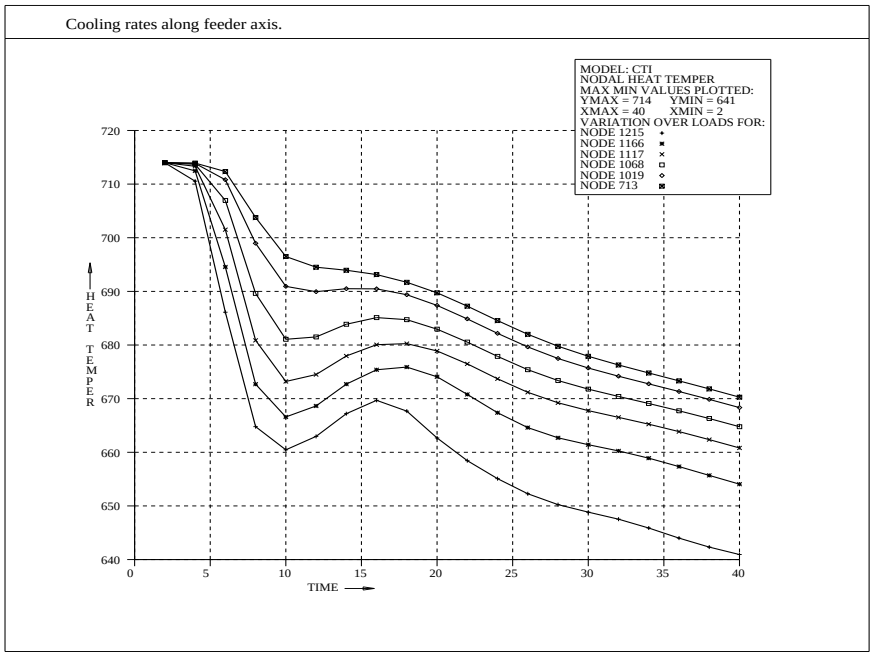

Figure 7.28: Cooling rates at various nodal points on the feeder axis.

with regard to the mould have been satisfied so far.

The thermo-mechanical analyses with and without natural convection are illustrated in Figures 7.37, 7.38, 7.39 and 7.40. After 100 seconds no mechanical effects are observable in either case as expected. After 300 seconds considerable stress effects are observable in the thermo-mechanical analysis without natural convection, but no observable stress effects are occurring in the thermo-mechanical analysis with natural convection included. This is attributable to the different cooling rates of the sprue and test bar that can be observed between the two analyses. It can be assumed that similar stress effects will occur in the latter thermo-mechanical analysis at a later stage in the analysis. Indeed, though not observable in Figure 7.39, small initial stress effects are present.

The stresses and inelastic strains agree physically with the deformation illustrated in Figure 7.36, where the casting is free to contract no stresses will occur, but where the casting is constrained by the mould stresses and inelastic strains will occur as illustrated in Figures 7.40 and 7.42.

With regard to gap formation at the casting/mould interface, the cooling rates are affected in both the thermo-mechanical analyses as illustrated by comparing Figures 7.33 and 7.34 with Figures 7.39(1) and 7.40(1), respectively. Though it should be noted that the effect of gap formation on the cooling rate requires further validation against experimental results with regard to sand casting.

Finally, it was interesting to compare a rate dependent and rate independent analysis. The results are illustrated for thermo-mechanical analyses without natural convection in Figures 7.38, 7.40, 7.41 and 7.42. The stresses in the rate dependent analysis are much higher and the associated visco-plastic strains are much lower. This agrees physically with rate dependent phenomena as the associated stresses are allowed to exist above the yield stress and the visco-plastic strain is limited by the time interval associated with the mechanical analysis.

It is interesting to note the occurrence of rate dependent effects in the sand casting problem and not in the previous die casting problem, this can be attributed to the different cooling rates associated with both problems. The die casting cools relatively quickly and in a uniform manner, whereas the sand casting cools slowly and in a non-uniform manner. The initial conclusions with regard to the occurrence of rate dependent material behaviour exhibited in the casting of metals are tentative and further research combined with experimental validation must be performed to reinforce these conclusions further.

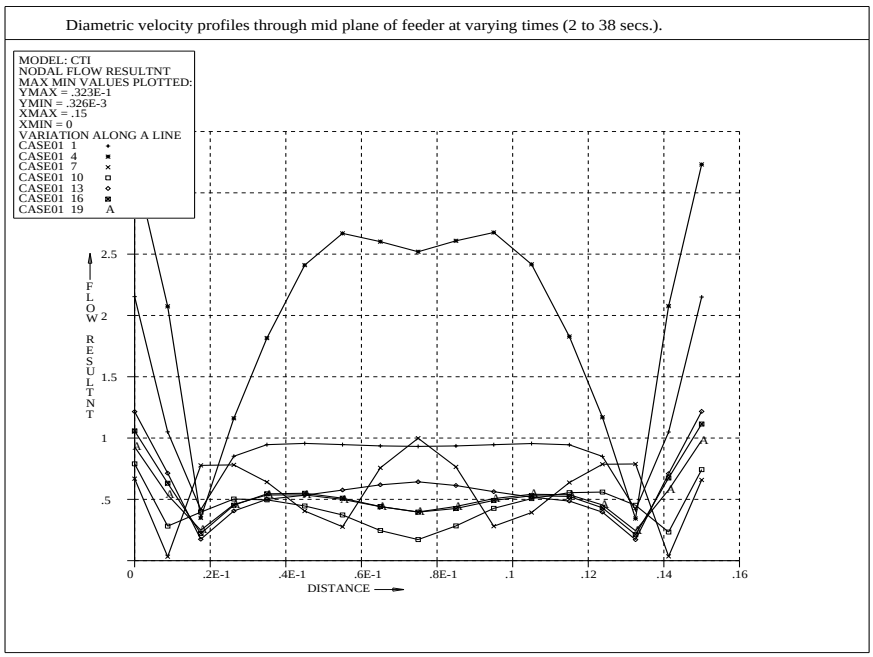

Figure 7.29: Velocity profiles along the diameter of the mid plane of the feeder.

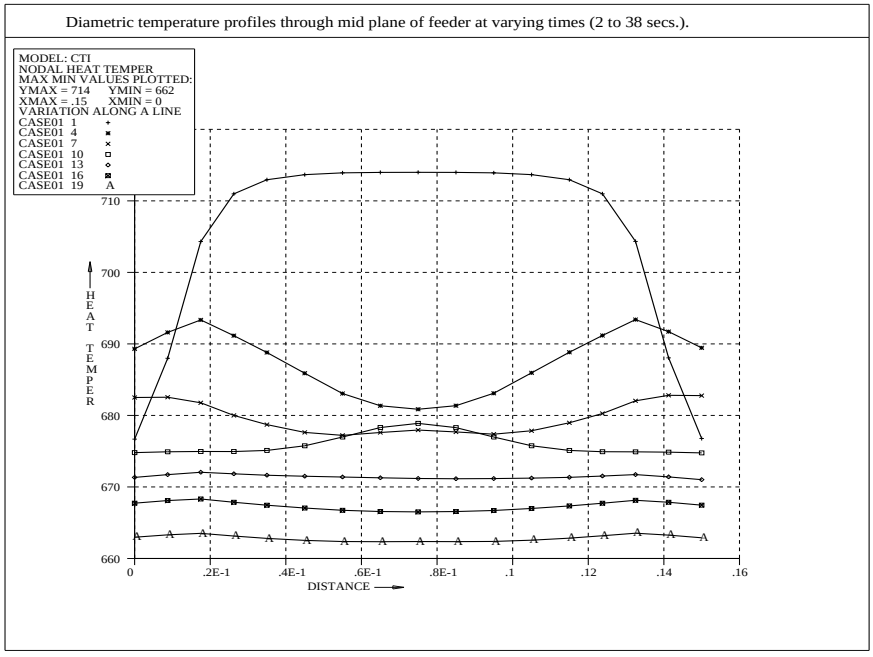

Figure 7.30: Temperature profiles along the diameter of the mid plane of the feeder.

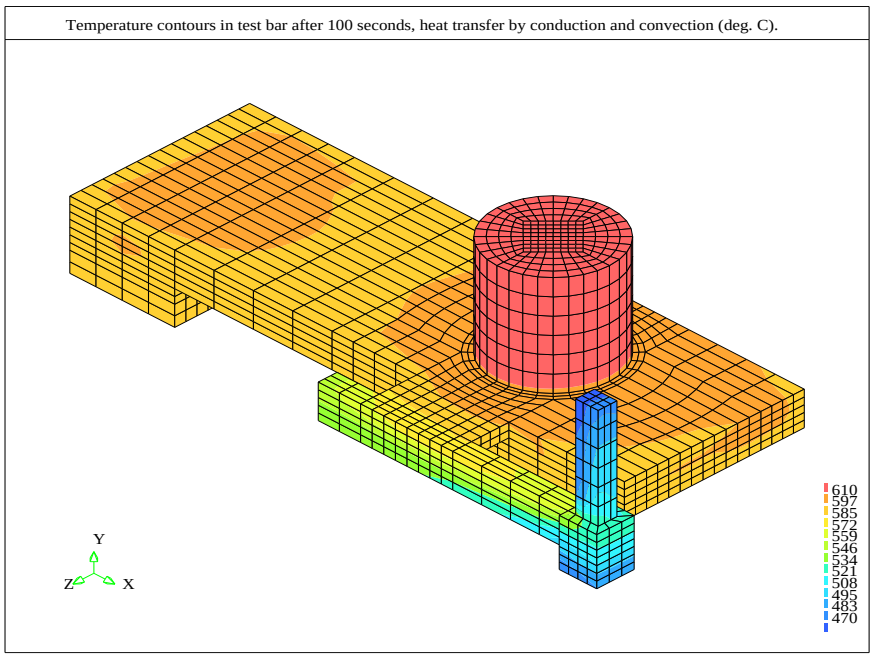

Figure 7.31: Heat transfer by conduction and convection after 100 seconds.

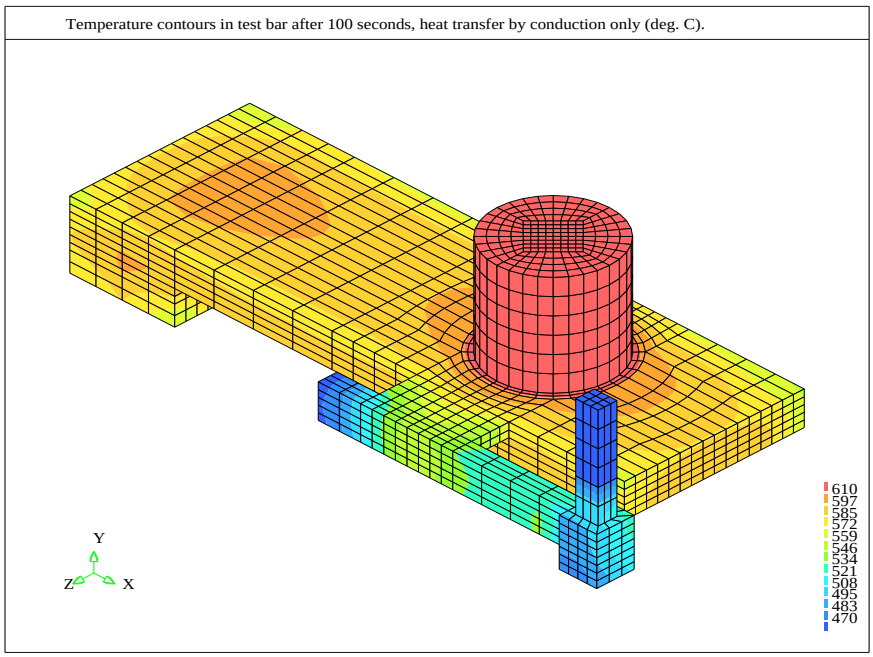

Figure 7.32: Heat transfer by conduction only after 100 seconds.

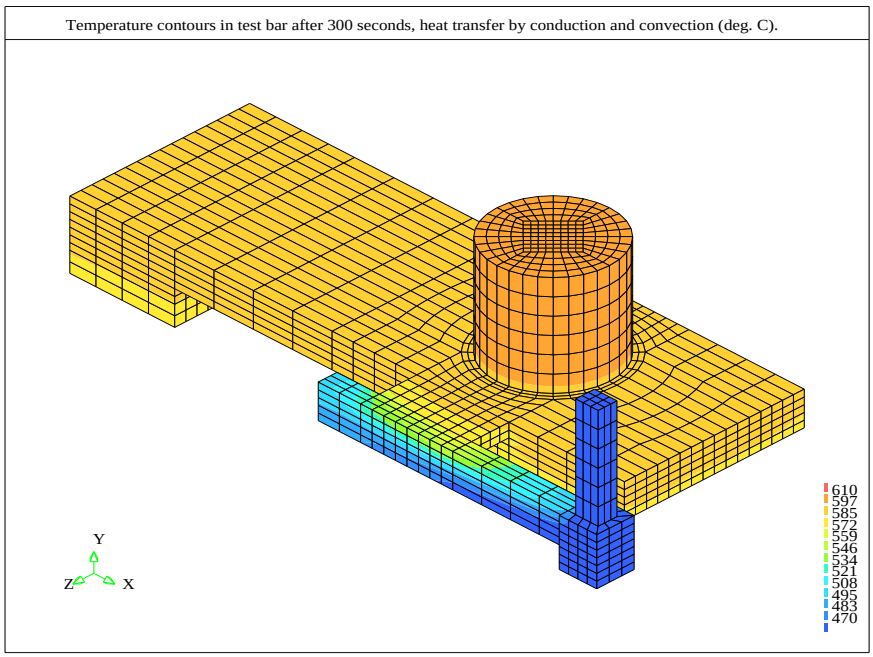

Figure 7.33: Heat transfer by conduction and convection after 300 seconds.

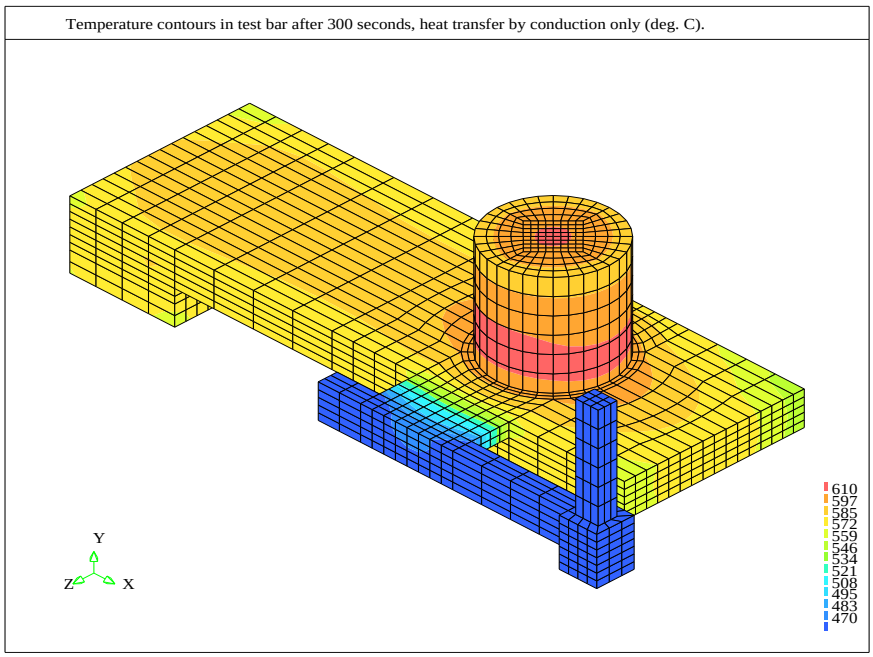

Figure 7.34: Heat transfer by conduction only after 300 seconds.

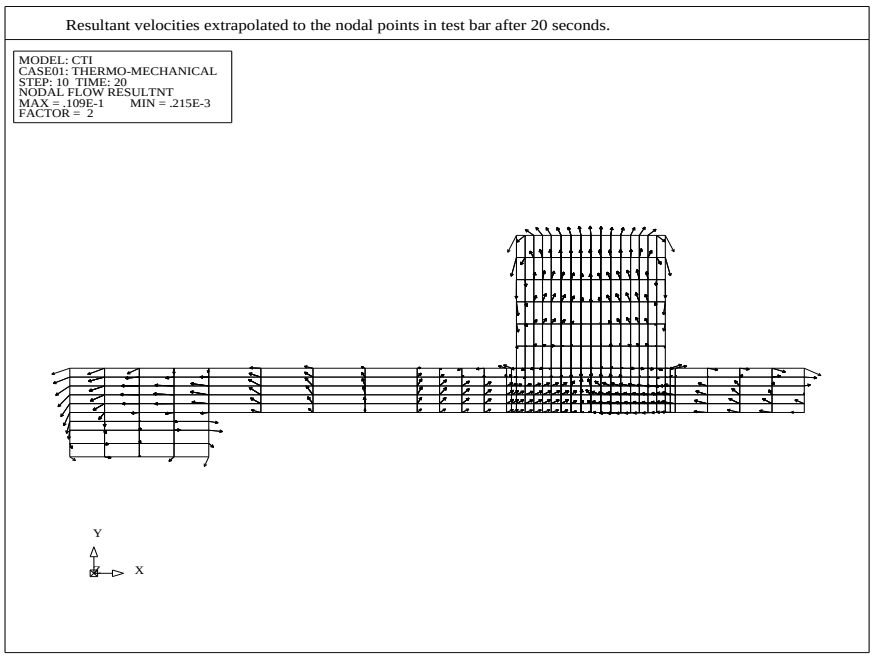

Figure 7.35: Resultant liquid velocity through a cross section at 20 seconds.

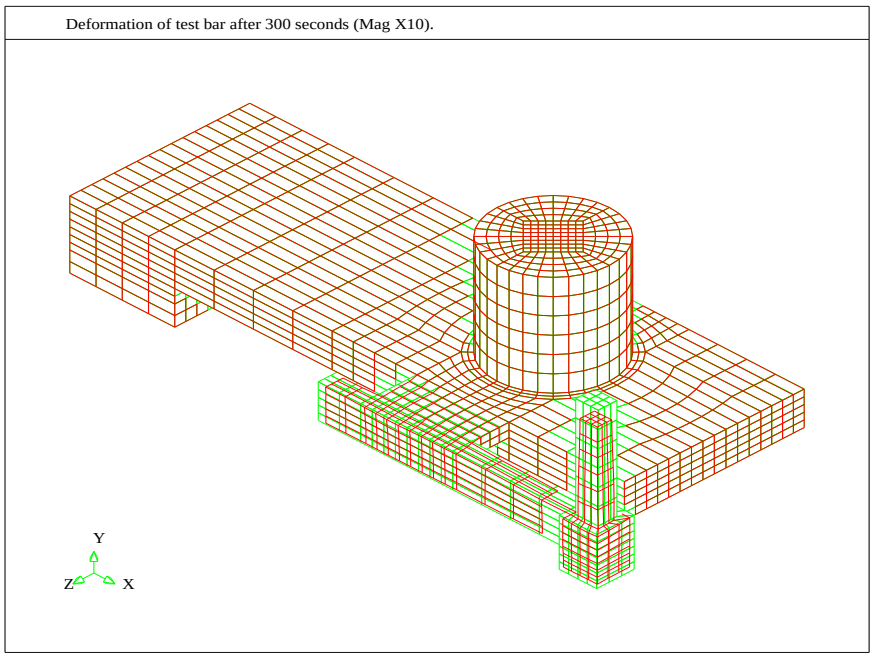

Figure 7.36: Deformation of the test bar after 300 seconds.

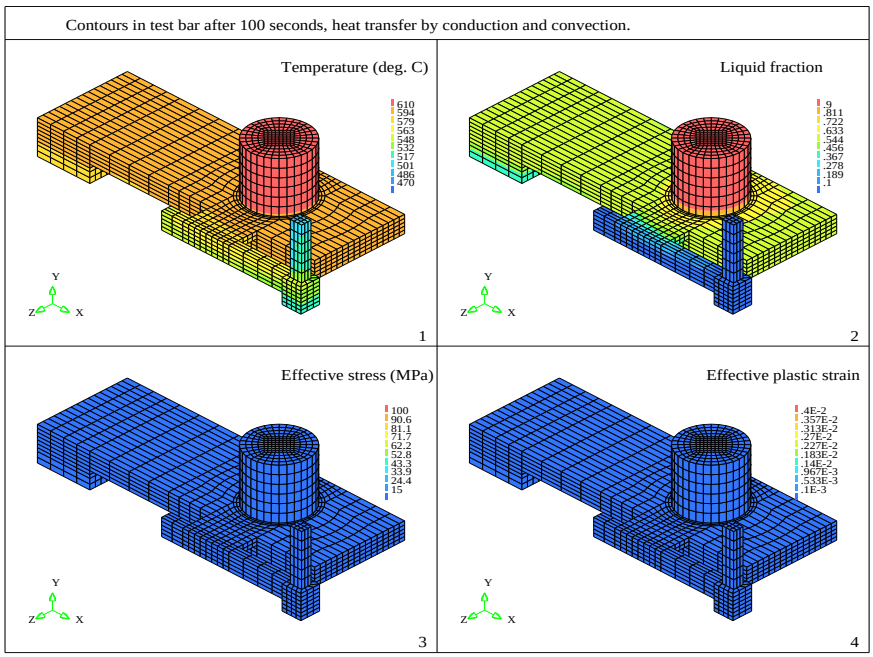

Figure 7.37: Thermo-mechanical behaviour after 100 seconds, heat transfer with convection.

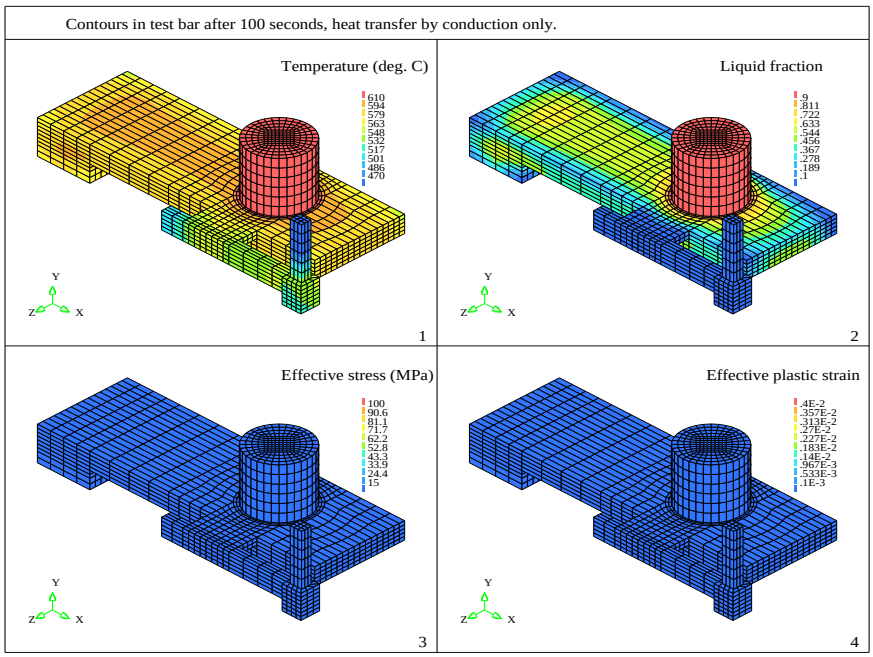

Figure 7.38: Thermo-mechanical behaviour after 100 seconds, heat transfer without convection.

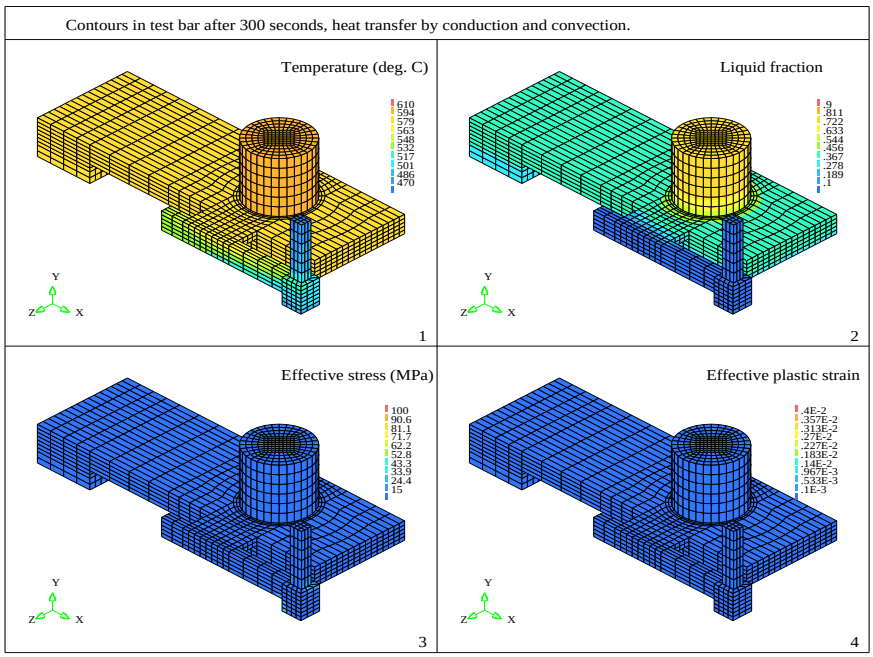

Figure 7.39: Thermo-mechanical behaviour after 300 seconds, heat transfer with convection.

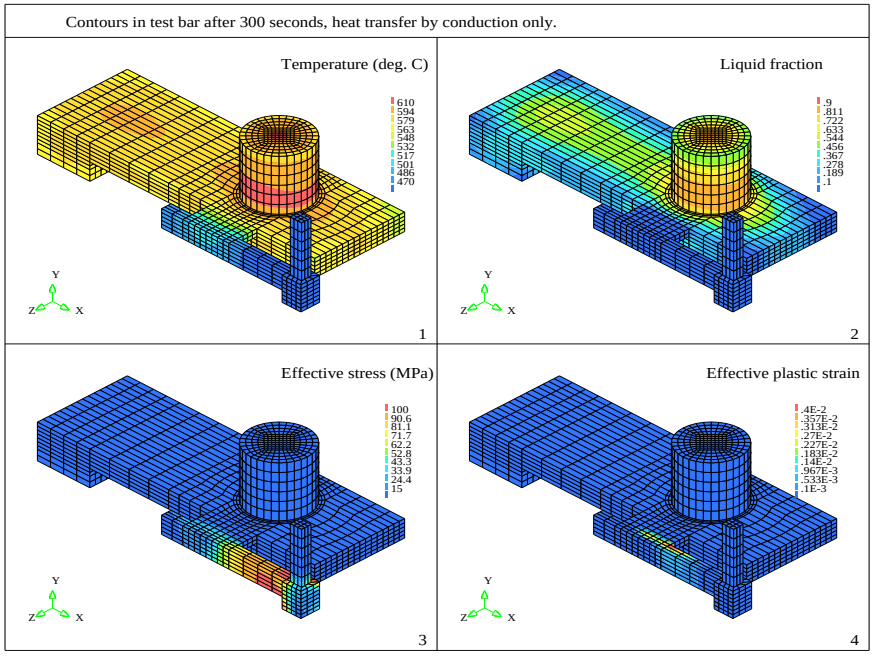

Figure 7.40: Thermo-mechanical behaviour after 300 seconds, heat transfer without convection.

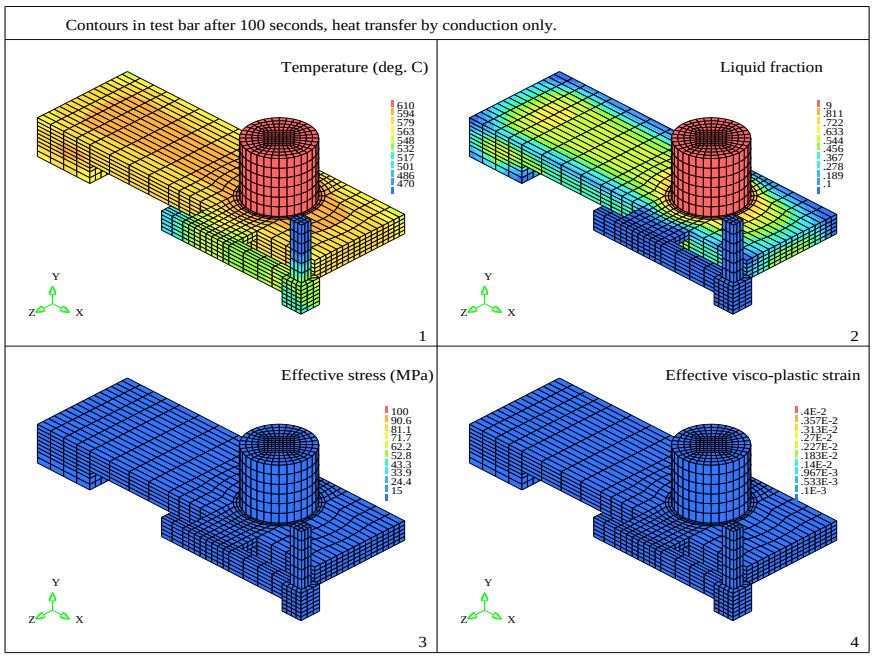

Figure 7.41: Rate dependent thermo-mechanical behaviour after 100 seconds.

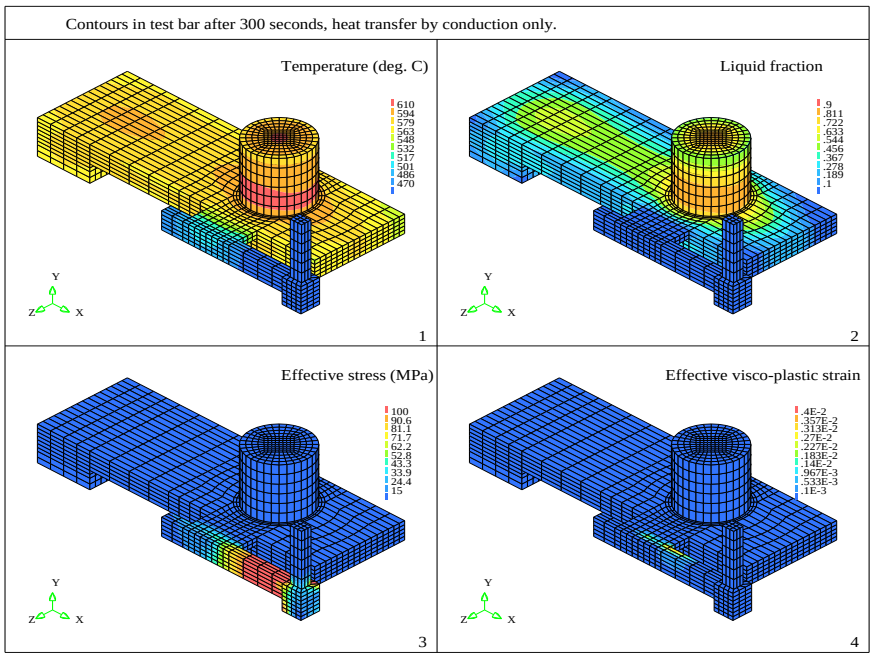

Figure 7.42: Rate dependent thermo-mechanical behaviour after 300 seconds.

7.4 Closure

In this chapter the capability of the FV framework PHYSICA to simulate the shape casting of metals has been illustrated and the importance of a fully coupled thermo-mechanical analysis has been demonstrated.

Initially, the die casting of an aluminium cylinder was simulated as a validation problem and the consequential results compared well against those of the experimental analysis. The comparison can be improved immediately by extending the PHYSICA framework to include a latent heat to solid fraction relationship suitable for binary alloys and a deformable-deformable contact algorithm to furnish mould dilation.

Finally, the sand casting of an aluminium test bar was simulated as an academic problem and the consequential results provided an illustration of both the full capability and present limitations of the PHYSICA framework with regard to the shape casting of metals. The sand casting problem illustrates interesting results from the inclusion of natural convection and rate dependent material behaviour in the thermo-mechanical analysis. Additionally, the problem illustrated the necessity for a robust contact algorithm and for the optimisation of the CSM algorithms with regard to computational effort.